Journal of Quantitative Spectroscopy & Radiative Transfer 251 (2020) 107027

Contents lists available at ScienceDirect

Journal of Quantitative Spectroscopy & Radiative Transfer

journal homepage: www.elsevier.com/locate/jqsrt

Empirical rovibrational energy levels of ammonia up to 7500 cm^{-1}

Tibor Furtenbacher[a], Phillip A. Coles[b], Jonathan Tennyson[b], Sergei N. Yurchenko[b], Shanshan Yu[c], Brian Drouin[c], Roland Tóbiás[a], Attila G. Császár[a,*]

[a] MTA-ELTE Complex Chemical Systems Research Group and ELTE Eötvös Loránd University, Institute of Chemistry, Laboratory of Molecular Structure and Dynamics, H-1117 Budapest Pázmány Péter sétány 1/A, Hungary
[b] Department of Physics and Astronomy, University College London, London WC1E 6BT, United Kingdom
[c] Jet Propulsion Laboratory, California Institute of Technology, Pasadena, CA 91109, USA

ARTICLE INFO

Article history:
Received 7 March 2020
Revised 10 April 2020
Accepted 10 April 2020
Available online 20 April 2020

Keywords:
Ammonia ($^{14}NH_3$)
Rovibrational transitions
Empirical rovibrational energy levels
MARVEL
Database
Spectroscopic networks
Effective Hamiltonian fits

ABSTRACT

The most recent version of the MARVEL (Measured Active Rotational-Vibrational Energy Levels) protocol and code is used to update and extend the list of accurately known empirical rovibrational energy levels of $^{14}NH_3$ falling in the range of 0 – 7500 cm^{-1}. Compared to an earlier similar study covering all the measured transitions of $^{14}NH_3$ [22], the present investigation is limited to transitions with an upper energy level below 7500 cm^{-1}, considers 82 sources (28 new) of transitions data, corrects several older assignments, and utilizes an improved validation procedure based partially on high-quality first-principles rovibrational energies. This study yields 4936 uniquely labelled empirical rovibrational energy levels, the set is complete up to 2413 cm^{-1}. We confirm the overall high accuracy of the most recent "spectroscopic" (fitted) $^{14}NH_3$ potential energy surface, C2018, up to 7500 cm^{-1}. Investigation of energy values resulting from previous effective-Hamiltonian fits forms an important part of this study. It is established that previous effective-Hamiltonian fits, using high expansion orders in the Hamiltonian, are inaccurate for certain high rotational excitations of all vibrational parents considered. Employing the ground vibrational state as a test case, it is shown that the origin of the problem is that the observed $^{14}NH_3$ spectroscopic network formed by rotational transitions and used for the effective-Hamiltonian fit contains floating components. A much improved effective-Hamiltonian fit is presented whereby the floating components are connected to the principal components of the spectroscopic network by carefully selected first-principles links. It is recommended that for all molecules the experimental set of transitions employed for an effective Hamiltonian fit should be checked for floating components and extra care be exercised if they exist, as in these cases the adequate reproduction of the transitions does not automatically mean that the energies derived from the effective-Hamiltonian parameters are correct as well. The connectivity problem of measured spectroscopic networks becomes more and more pronounced as the order of the Hamiltonian is increased.

1. Introduction

Ammonia, NH_3, a simple four-atomic "inorganic" molecule, is vital to society as modern food production is highly dependent upon ammonia-based fertilizers. Ammonia is manufactured at the prodigious global rate of about 5 tonnes per second. Ammonia is a poisonous gas both for humans and plants and its ever-increasing release into the earth's atmosphere has several undesirable consequences [1–3]. Thus, monitoring the concentration of ammonia in the atmosphere and understanding the associated nitrogen cycle [2] are important scientific and engineering objectives which can be supported by detailed, high-resolution spectroscopic investigations. Measurements of spatially resolved atmospheric concentrations of ammonia require reliable and extensive laboratory data, preferably with a complete coverage of the energies and transitions of the spectroscopic regions of interest.

Astronomically, ammonia was the first polyatomic molecule detected in interstellar space [4] and, due to its thermodynamic stability, it is one of the principal molecular carriers of nitrogen. Ammonia provides one of the most accurate "molecular thermometers" for the interstellar medium [5,6] and it is omnipresent in star-forming primordial gas clouds. Ammonia is well known in solar-system gas giants and has recently been detected in the

* Corresponding author.
E-mail address: csaszar@chem.elte.hu (A.G. Császár).

https://doi.org/10.1016/j.jqsrt.2020.107027

atmosphere of a hot-Jupiter exoplanet [7]. Ammonia is thought to provide the key signature of Y-dwarfs [8,9], the coolest category of brown-dwarf stars. Consequently, ammonia spectra have been analysed in considerable detail in brown dwarfs [10]. Detailed knowledge of the high-resolution spectrum of ammonia at widely different temperatures, from cold (10 K) to hot (2000 K), is key to the success of a large number of astronomical studies.

The rovibrational states of ammonia display characteristic and highly varying tunnelling splittings associated with ammonia's famous inversion motion [11–13]. Note that the splittings and the associated nuclear dynamics can be controlled by medium-intensity laser light [14], with possible technological applications [15]. The high-resolution rovibrational spectrum of ammonia is also relevant for metrology. Metrology studies based on precision spectroscopy and involving ammonia include the accurate determination of the Boltzmann constant [16–18] as well as the time variation of the electron-to-proton mass ratio [19–21].

Al-Derzi et al. [22] undertook a systematic compilation of a large number of measured and assigned high-resolution spectra of $^{14}NH_3$, published prior to 2014. The experimental transitions data collated by Al-Derzi et al. [22] determine 4961 empirical rovibrational energy levels. These levels were derived *via* the MARVEL (Measured Active Rotational-Vibrational Energy Levels) procedure [23–25], built upon the concept of spectroscopic networks [26–28]. The results of the investigation of Al-Derzi et al. [22] have been used for a number of scientific studies, including ones focused on nuclear-quadrupole coupling [29] and quadrupole splittings [30]. Since 2014, a number of new high-resolution studies of ammonia spectra have become available [30–41]. In addition, analysis of near-infrared (NIR) ammonia spectra [41] indicated that a number of transitions included in the study of Al-Derzi et al. [22] were not assigned entirely correctly, which, combined with some other issues [13], led to a number of incorrect or incorrectly assigned energy levels. A number of changes to the transitions data collated by Al-Derzi et al. [22] have already been described in Ref. [13]. For these changes the reader should consult the Supplementary Material of Ref. [13].

As part of this work, we extend and update the MARVEL analysis of the high-resolution spectra of $^{14}NH_3$. In doing so we use not only new [30–41] and re-assigned spectra but have taken the opportunity to include several older sources of spectroscopic data [42–64], which, for various reasons, were not treated by Al-Derzi et al. [22]. As a result, the current MARVEL database contains considerably more measured transitions than that employed by Al-Derzi et al. [22].

A significant portion of the recent experimental studies have concentrated on vibration-rotation spectra of ammonia with transitions above 7000 cm^{-1} [35,39–41]. Two of these investigations, Refs. [35] and [39], represent the first ever assignment of the 7400–8600 and the 9000–11 000 cm^{-1} regions. A recent study [41] found certain discrepancies between the assignments of Ref. [41] and Ref. [35]. It would therefore not be surprising if similar issues with the assignments presented in Ref. [39] appeared in the future. Until more work is done to consolidate the results of Refs. [35] and [39], it is safest not to include them in a MARVEL-based study. Thus, we restrict the present investigation to transitions lying below 7500 cm^{-1}. Al-Derzi et al. [22] considered only a single source which contained transitions above 6625 cm^{-1}. This source, 86CoLe [65], contains 323 partially assigned lines lying at about 15 000 cm^{-1}. These results have recently been reassessed by Zobov et al. [40] and the reader is referred to Ref. [40] for further information on observed high-resolution ammonia spectra at visible wavelengths. They will not be discussed further in this paper.

A number of variationally computed line lists are available for ammonia [40,66–70]. These can be highly useful for validating the empirical energy levels produced by the MARVEL procedure. In this study we employ the recent C2018 [70] and CoYuTe [71] variational line lists for validation purposes. The C2018 line list, which was produced as part of the ExoMol project [72,73], is significantly more accurate than the BYTe line list [67] used for validation of the empirical rovibrational energy levels deduced by Al-Derzi et al. [22]. Overall, one of the principal aims of the present study is the production of a set of assigned rovibrational energy levels of $^{14}NH_3$ up to 7500 cm^{-1} containing as many accurate empirical levels as possible. When empirical energy levels are not available, we recommend the complete set of first-principles energy levels of Ref. [71]. Accuracy of the complete energy level set of a molecule could be improved by replacing first-principles energy values with those derived from effective Hamiltonians (EH). However, in the case of $^{14}NH_3$, as shown below, one must be particularly careful with this approach.

Historically, EHs have been considered [74–79] unsuitable for fitting the observed high-resolution spectra of ammonia to experimental accuracy. Nevertheless, recent studies by Pearson and co-workers [33,80–82] showed that carefully constructed rotation-inversion EHs are capable of describing most of the measured transitions with remarkable accuracy. The vibrational states for which rotation-inversion EHs are available include the non-interacting ground and ν_2 states, as well as the $2\nu_2-\nu_4$ and $3\nu_2-(\nu_2+\nu_4)$ pairs (we employ the canonical ordering of the vibrational states throughout this paper). While it is expected that EHs may not be able to extrapolate properly, it is usually assumed that they do interpolate energy levels with an accuracy that surpasses significantly that of even the best first-principles variational computations. Thus, we decided to investigate how best to complement empirical rovibrational energies of $^{14}NH_3$ with EH ones in order to improve the accuracy of the final energy levels set of this study. The task is especially hard for high-K states for which characteristics of the ammonia spectroscopy, in particular the $\Delta K=0$ propensity rule, make the fitting particularly challenging. As detailed in Section 3, we found significant issues with the EH fits of Refs. [33,80–82]. New EH fits, yielding much more accurate rovibrational energy values for certain highly excited rovibrational states have been made and a new set of spectroscopic parameters is provided for the vibrational ground state of $^{14}NH_3$.

2. Empirical rovibrational energy levels of $^{14}NH_3$

The MARVEL protocol [23–25], yielding empirical rovibrational energies, always starts with the construction of a spectroscopic network (SN) [26,28] for the molecule in question, here $^{14}NH_3$, using the dataset of measured and assigned transitions collated from the literature. The measured transitions must each have a *unique* assignment, which determines their place within the SN, and an uncertainty. An inversion is then performed, yielding empirically determined rovibrational energy levels within each component of the SN. Recently the algorithms employed by MARVEL have been systematically improved [23,25,83], the relationship of SNs to formal network theory considered [26,27,84], and the underlying methodology reviewed [28,85,86]. MARVEL has been used to obtain accurate empirical rovibronic energy levels for a considerable number of molecules, including diatomic [87–91], triatomic [92–101], tetratomic [22,102], and polyatomic [103] species.

NH_3 has three identical H atoms whose interchange is therefore subject to the Pauli principle. Within the D_{3h}(M) molecular-symmetry (MS) group [104], the states are divided into three categories: *ortho* states have (A_2',A_2'') symmetry, *para* states have (E',E'') symmetry, and there are no states of (A_1',A_1'') symmetry. The hypothetical lowest-energy state of $^{14}NH_3$, with all quanta being zero, has A_1' symmetry. Thus, it is a "missing" state. The *ortho* and *para* nuclear-spin isomers are not linked by any transitions and therefore form distinct (so-called principal) components (PC). The PCs

of the SN can be linked by what we call a "magic number". In this study, the lowest *ortho* energy level [$(v_1\ v_2\ v_3^{l_3}\ v_4^{l_4})\ J\ K\ inv = (0\ 0\ 0^0\ 0^0)\ 1\ 1\ s$, see below for the meaning of the label] is fixed to 16.172 993 cm^{-1}, while the energy of the lowest *para* level, $(0\,0\,0^0\,0^0)\,0\,0\,a$, is fixed to 0.793 403 cm^{-1}. Both of these values are taken from Ref. [105]. Note that future improvements of ammonia spectroscopy may result in changes in these values, similar to what happened to the "magic number" of $H_2{}^{16}O$ [106].

2.1. State labeling

In the study of Al-Derzi et al. [22] each rovibrational eigenstate of $^{14}NH_3$ was represented by the following set of 12 descriptors: $[v_1\ v_2\ v_3\ v_4\ l_3\ l_4\ J\ K\ inv\ \Gamma_{rot}\Gamma_{vib}\ \Gamma_{tot}]$, where v_i $(i = 1, \ldots, 4)$ are the vibrational normal-mode quantum numbers (employing canonical ordering), l_3 and l_4 are the vibrational angular-momentum quantum numbers associated with modes 3 and 4, respectively, J is the total angular-momentum quantum number, $K = |k|$ is the projection of the total angular momentum on the molecule-fixed axis z, and $inv = a/s$ is the inversion symmetry (asymmetric/symmetric or odd/even) of the vibrational motion. In the MARVEL database of Al-Derzi et al. [22], 0 represents the symmetric/even, while 1 the asymmetric/odd choice, while in this study we use s for the symmetric and a for the asymmetric inversion. The last three descriptors of the label provide the rotational (Γ_{rot}), the vibrational (Γ_{vib}), and the full (Γ_{tot}) symmetry of the eigenstate. This information comes from sophisticated quantum-chemical computations of the rovibrational levels and helps when matching empirical energy levels with their first-principles counterparts.

In 2016, several labeling problems of the database of Al-Derzi et al. [22] related to the sign of l_3 and l_4 were identified and corrected by two of the present co-authors [13]. Determination of the sign of l_i is almost impossible, especially in highly-excited cases. Therefore, the L_3 and L_4 values were introduced as quantum numbers used in the label, where $L_i = |l_i|$, as had been recommended previously [107]. During the present study we decided to employ the L_i labels and add an index (or counting number) for levels within each $J - \Gamma_{tot}$ block of the CoYuTe [71] energy list, N_{block}, to the set of descriptors, since (a) the block index is unique, (b) determination of N_{block} is a preliminary test whether the given empirical energy level exists in the first-principles energy list or not, and (c) this index facilitates the straightforward matching with first-principles energy lists [67,68,108]. At the same time, we remove the redundant Γ_{rot} and Γ_{vib} labels. Thus, in the present MARVEL database of $^{14}NH_3$ the following 11 descriptors identify a rovibrational state: $[v_1\ v_2\ v_3\ v_4\ L_3\ L_4\ J\ K\ inv\ \Gamma_{tot}\ N_{block}]$.

2.2. Experimental data sources

All sources of experimental rovibrational data collated by Al-Derzi et al. [22], Refs. [16,32,75–81,105,109–154], except 86CoLe [65] (because its wavenumber range begins at 15 259 cm^{-1}, above the range covered in this study), were retained in our compilation. Furthermore, we (re-)evaluated a number of older experimental sources, Refs. [42–64], not used in the final compilation of Al-Derzi et al. [22]. A number of new data sources [30,31,33,34,82] were also included in the revised set of experimental transitions. We ignored six new data sources [35,37–40,155] because either they deal with spectra at wavenumbers above 7500 cm^{-1} [35,39,40], thus they are irrelevant for the present study, or their resolution is not sufficient for our present purpose [37,38,155]. The very recent infrared transmission spectrum of hot ammonia reported by 20BeWoBe [156] was not considered as this source contains no line assignments.

Table 1 contains information about all the data sources included in our present compilation. It is important to reemphasize that the present MARVEL database contains only those experimentally measured lines in which both energy levels are under 7500 cm^{-1} and are connected to the PCs. As a result, the database assembled contains no floating components (FC). Thus, in this study the experimental SN of $^{14}NH_3$ contains 15 729 and 30 386 transitions in the *ortho* and *para* PCs, respectively. Table 2 shows the vibrational bands and the number of rovibrational states belonging to each vibrational band origin (VBO) included in the present MARVEL database.

The final MARVEL run of this study considered 46 115 transitions from 82 sources (28 new), of these 46 037 were validated. These lines determine 1753 *ortho* and 3183 *para* energy levels. Files containing our final transition set (wavenumbers of unvalidated lines are indicated with negative sign) and energy levels are deposited in the supplementary data and can also be found on the MARVEL website at http://kkrk.chem.elte.hu/marvelonline/molecules.php. By comparison, Al-Derzi et al. [22] validated 27 930 measured transitions characterized by energy values less than 7500 cm^{-1}. Overall, the number of energy levels already present in the analysis of Al-Derzi et al. [22] up to 7500 cm^{-1}, 4716, increases to 4936 at the end of the present study. Thus, although we treated 65% more transitions, the number of energy levels increased only marginally, by 5%. The 220 new energy levels come from only two sources, 146 from Ref. 15BaYuTeCl [32] and 74 from 16PeYuPi [33].

One of the most recent sources of $^{14}NH_3$ transitions, 16TwHaSe [30], reports 58 highly accurate lines, with uncertainties estimated to be 20–30 kHz, for the $\nu_1 + \nu_3$, $\nu_1 + 2\nu_4$, and $\nu_3 + 2\nu_4$ bands. Now, in the MARVEL world it often happens that different sources with about the same accuracy predict distinctly different empirical energies. However, it is unprecedented that a highly-accurate source is in conflict with other previous measurements and dependable first-principles results at the same time. Two lines of 16TwHaSe show such conflicts with the lines of 12SuBrHuSc [79], 07LiLeXu [145], and 14FoGoHeSo [135]. The first "problematic" line, at 6488.199 520 0 cm^{-1}, predicts an energy value of about 6951.907 cm^{-1} for the $(0\,0\,1^1\,2^2)\,6\,6\,a$ state, while the previous measurements suggest 6951.940 cm^{-1}. Note that basically the same conflict has already been noted in 12SuBrHuSc [79]. There two out of three relevant lines predicted an energy of 6951.940 cm^{-1}, while the third line yielded 6951.906 cm^{-1}. The second "problematic" line of 16TwHaSe is the one at 6508.300 271 2 cm^{-1}. This line corresponds to an energy of about 6673.631 cm^{-1} for the $(1\,0\,0^0\,2^2)\,3\,2\,s$ state, while the other measurements [135,145] yield 6672.711 cm^{-1}. Since the CoYuTe first-principles energy list seemingly supports the results of the older measurements, we tentatively deleted the two conflicting lines of 16TwHaSe mentioned from the final MARVEL analysis.

2.3. Comparison of empirical energy levels with first-principles data

Al-Derzi et al. [22] partially validated the empirical energy levels of $^{14}NH_3$ by comparing them with their counterparts in the BYTe variationally computed energy list [67]. The accuracy of variationally computed energies has recently been improved significantly with the production of a 'spectroscopic' potential energy surface (PES) called C2018 [70], produced by refining the high-accuracy *ab initio* PES of Polyansky et al. [157] to energies carefully selected from those produced by Al-Derzi et al. [22]. Since the energy list of C2018 contains energies only up to $J = 20$, during this study we utilized the extended version of this database, called CoYuTe [71], which provides energies up to $J = 43$. Nevertheless, one must emphasize that the fitting of the C2018 PES included empirical energies only up to $J = 8$ (to include any higher levels of rotational excitation would have been computationally too expensive).

Table 1
Characteristics of the experimental data sources of rovibrational transitions of $^{14}NH_3$ analyzed during the present study. *A* and *V* stand for the available (below 7500 cm^{-1}) and validated transition entries in a given segment, respectively. ESU, MSU, and LSU designate the estimated, the median, and the largest segment uncertainties, in cm^{-1}, respectively. Bold-face tag entries refer to sources not considered by Al-Derzi et al. [22]. The sources are listed according to their decreasing accuracy in column ESU, with the restriction that segments of the same source are listed consecutively.

Segment tag	Range	*A*/*V*	ESU	MSU	LSU
67Kukolich [43]	0.79036–0.79622	3/3	7.00e−09	7.00e−09	7.00e−09
70KuWo [44]	0.72395–0.81833	5/5	7.00e−09	7.00e−09	7.00e−09
09CaDoPu [64]	19.096–19.096	2/2	6.50e−09	6.50e−09	7.00e−09
65Kukolich [42]	0.76167–0.76167	1/1	1.70e−08	1.70e−08	1.70e−08
74CoPo [109]	0.68898–1.9580	50/50	1.67e−07	1.67e−07	1.33e−06
75PoKa [110]	0.24303–1.3323	119/119	1.67e−07	1.67e−07	3.88e−06
80SiSm [50]	0.18123–0.40734	15/15	3.34e−07	3.34e−07	3.34e−07
88TaEnHi [111]	10.670–11.077	14/14	5.31e−07	5.31e−07	5.43e−06
82SaHaAmSh [112]	2.2768–5.9274	12/11	6.67e−07	6.67e−07	6.67e−07
96WiBeKlUr [62]	38.975–40.536	3/3	6.70e−07	6.70e−07	6.70e−07
16TwHaSe [30]	6487.8–6636.7	58/56	6.67e−07	6.67e−07	1.67e−06
98FiKhRuLe [113]	967.25–967.25	1/1	8.74e−07	8.74e−07	8.74e−07
90SmFiDa [60]	0.33685–1.5385	14/14	1.30e−06	1.30e−06	3.15e−06
80Cohen [114]	2.0862–4.0680	17/17	2.34e−06	2.34e−06	6.67e−06
92SaEnHiPo [75]	2.3527–1387.9	80/80	2.00e−06	2.00e−06	1.89e−05
92SaEnHiPo_S2 [75]	1388.1–1859.7	727/727	2.00e−04	2.00e−04	2.33e−02
10YuPeDrSu [81]	13.334–157.19	175/175	1.70e−06	1.70e−06	6.32e−05
10YuPeDrSu_S2 [81]	39.080–672.64	1600/1600	3.00e−04	3.00e−04	1.73e−02
84MaScFrKr [55]	934.38–1075.2	9/9	3.30e−06	3.30e−06	1.30e−05
08SuLeXu [63]	1027.0–1075.2	14/14	3.34e−06	3.34e−06	1.43e−05
11DrYuPeGu [115]	84.014–89.042	5/5	3.30e−06	3.30e−06	3.30e−06
11LeTrDaBo [16]	965.79–965.79	1/1	3.34e−06	3.34e−06	3.34e−06
06ChPePiMa [80]	15.552–46.468	30/30	3.80e−06	3.80e−06	6.21e−05
96KrTrBoBa [116]	40.523–40.536	2/2	5.30e−06	5.30e−06	5.94e−06
16PeYuPi [33]	13.722–90.955	159/159	6.70e−06	6.70e−06	6.05e−05
16PeYuPi_S2 [33]	39.554–707.26	1221/1221	6.00e−04	6.00e−04	3.81e−02
16PeYuPi_S3 [33]	61.937–682.28	1470/1470	1.00e−03	1.00e−03	3.92e−02
98BeUrWi [117]	4.6746–25.446	3/3	1.11e−05	1.11e−05	2.85e−05
00UrHeKhFi [118]	948.23–951.78	2/2	1.33e−05	1.33e−05	2.64e−05
85SiRe [56]	788.51–1084.6	15/15	1.74e−05	1.74e−05	6.81e−05
80BeGeKrMa [49]	4.6747–35.793	55/55	3.34e−05	3.34e−05	3.13e−04
11GuJeMoPe [119]	1126.0–1171.4	22/22	4.00e−05	4.00e−05	1.75e−04
82MiToCaLi [52]	1084.6–1084.6	5/5	6.66e−05	6.66e−05	1.09e−04
85BrTo [120]	814.24–1122.1	81/81	7.00e−05	7.01e−05	3.01e−04
86SaScMaPo [121]	772.44–1157.4	138/138	6.79e−05	6.79e−05	1.58e−03
89UrTuRaGu [122]	3984.9–4648.0	785/785	9.00e−05	9.00e−05	9.37e−04
89UrTuRaGu_S2 [122]	3982.8–4633.1	74/74	2.61e−03	2.61e−03	9.58e−03
89UrTuRaGu_S3 [122]	3969.9–4658.6	32/32	1.41e−02	1.41e−02	3.76e−02
77KoMuHiBu [47]	887.88–971.88	11/11	1.41e−04	1.41e−04	3.40e−04
83PoMa [54]	19.096–316.78	204/204	1.28e−04	1.28e−04	4.36e−03
81SaMiWo [123]	932.88–1084.6	32/32	2.00e−04	2.00e−04	8.16e−03
81SaWo [51]	924.95–1043.1	39/39	2.00e−04	2.00e−04	2.00e−04
83ShBjSc [53]	891.88–1103.5	88/88	2.00e−04	2.00e−04	1.17e−03
83UrPaKaYa [124]	709.09–1158.7	640/640	2.00e−04	2.00e−04	2.09e−02
84PoMa [125]	723.27–1250.2	533/533	2.00e−04	2.00e−04	1.03e−02
94ChChCh [126]	928.56–955.06	48/48	2.00e−04	2.00e−04	7.36e−04
95FaItYa [61]	904.80–1178.8	133/133	2.00e−04	2.00e−04	7.88e−03
76FrOk [45]	926.05–1084.6	56/55	2.65e−04	2.65e−04	3.88e−03
79HiJeFa [127]	949.45–949.45	1/1	4.10e−04	4.10e−04	4.10e−04
95KlTaBr [76]	429.37–3114.8	2066/2062	4.00e−04	4.00e−04	3.95e−02
18PeYuPeSu [82]	16.068–1572.8	1266/1266	4.16e−04	4.16e−04	3.07e−02
77HiKoBuFa [46]	887.88–1027.0	9/9	5.00e−04	5.00e−04	6.70e−04
81UrSpPaKa [128]	4.6747–969.02	299/299	4.70e−04	4.70e−04	2.18e−02
84Weber [129]	1511.3–1880.3	176/176	5.00e−04	5.00e−04	8.08e−03
87DCunha [57]	701.46–1187.4	196/196	5.00e−04	5.00e−04	1.72e−02
87LeLaGuTa [58]	1800.0–2099.4	455/455	5.00e−04	5.00e−04	2.49e−02
89GuAbTuRa [130]	3023.3–3674.9	1382/1380	5.00e−04	5.00e−04	2.91e−02
93PiDa [131]	3331.0–3415.4	100/100	5.00e−04	5.00e−04	3.23e−03
96BrMa [132]	4802.2–5293.0	615/610	5.00e−04	5.00e−04	3.15e−02
99FaYa [133]	770.91–1178.8	126/126	5.00e−04	5.00e−04	2.21e−03
99KlBrTaKo [134]	2980.4–3633.8	2162/2162	5.00e−04	5.00e−04	5.21e−02
00CoKlTaBr [77]	1333.0–2096.1	1202/1202	5.00e−04	5.00e−04	2.65e−03
01CoTaKlBr [78]	1201.9–2749.2	1305/1305	5.00e−04	5.00e−04	4.32e−02
13ArMaBo [31]	991.69–1859.7	462/462	5.00e−04	5.00e−04	5.96e−03
14FoGoHeSo [135]	6410.3–6764.5	212/209	5.00e−04	5.00e−04	3.62e−02
86UrCuMaRa [136]	511.37–1347.8	579/579	5.77e−04	5.77e−04	4.15e−02
84UrCuNaPa [105]	1167.9–2126.7	950/949	6.60e−04	6.60e−04	3.74e−02
78Nereson [137]	942.57–956.15	27/27	8.11e−04	8.11e−04	3.95e−03
86PaUrSpRa [138]	1425.8–1892.2	73/70	7.64e−04	7.64e−04	7.71e−03
94BrPe [139]	38.976–3415.1	174/174	9.07e−04	9.07e−04	2.80e−03

(*continued on next page*)

Table 1 (*continued*)

Segment tag	Range	*A*/*V*	ESU	MSU	LSU
78Jones [48]	887.88–1032.1	23/23	1.00e−03	1.00e−03	3.09e−03
85AnFiFrIl [140]	3134.6–3620.2	615/615	1.37e−03	1.37e−03	3.70e−02
11ZoShOvPo [141]	779.56–2029.2	5915/5900	1.00e−03	1.00e−03	8.19e−02
12SuBrHuSc [79]	6346.8–6973.5	1072/1057	1.00e−03	1.00e−03	4.00e−02
13DoHiYuTe [142]	0.42742–4810.6	10 661/10 657	1.00e−03	1.00e−03	6.27e−02
14CeHoVeCa [143]	4275.4–4339.7	229/228	1.00e−03	1.00e−03	3.89e−02
16SuYuPePi [34]	50.711–657.78	1725/1724	1.00e−03	1.00e−03	3.37e−02
86HeBiBa [144]	620.57–739.44	223/223	1.81e−03	1.81e−03	1.25e−02
07LiLeXu [145]	6421.2–6678.0	97/97	2.00e−03	2.00e−03	3.88e−02
08LeLiXu [146]	6440.0–6832.3	222/221	2.00e−03	2.00e−03	2.13e−02
14DiMiQuSc [147]	3355.0–3355.0	1/1	3.00e−03	3.00e−03	3.00e−03
80UrSpPaMc [148]	678.38–2014.0	482/481	3.91e−03	3.91e−03	5.00e−02
71HeDeGo [149]	19.885–19.885	1/1	5.26e−03	5.26e−03	5.26e−03
85UrMiRa [150]	3148.2–4503.7	478/478	5.00e−03	5.00e−03	3.94e−02
88SnBa [59]	931.18–932.14	7/7	5.00e−03	5.00e−03	5.00e−03
93LuHeNi [151]	6405.5–6887.9	315/314	5.33e−03	5.33e−03	1.70e−02
10PeHa [152]	6460.4–6541.4	16/16	5.00e−03	5.00e−03	1.06e−02
99BePeMe [153]	6540.2–6624.5	27/27	6.14e−03	6.14e−03	1.09e−02
15BaYuTeCl [32]	500.53–1883.7	1366/1349	1.36e−02	1.36e−02	8.08e−02

Fig. 1 shows the differences between the MARVEL and the CoYuTe [71] energies. As seen there, almost all MARVEL energy levels are reproduced by CoYuTe within 0.5 cm^{-1}, proving the high accuracy of the underlying PES. Residuals larger than this are typically associated with the CoYuTe vibrational labels of $2\nu_2+3\nu_4$, $4\nu_4$, $\nu_1+\nu_3$ or $4\nu_2+2\nu_4$, which are sometimes in conflict with the labels used in the present MARVEL dataset.

2.4. Comparison of empirical energy levels with existing EH data

Besides the (complete) set of first-principles rovibrational energies, EH energies, characterizing just one or a few vibrational bands, can also be used for validating empirical rovibrational energies derived during a MARVEL analysis. Thus, we employed the EH energy levels of 18PeYuPeSu [82] to check the MARVEL results of this study. As clearly seen in Fig. 2, on the vibrational ground state most of the MARVEL levels can be reproduced by the EH results within 0.005 cm^{-1}. Nevertheless, there are two sets of energy levels where the differences are significantly larger (about 0.015 and 0.15 cm^{-1}). Checking the experimental transitions we could not explain this unusual behavior. Therefore, we decided to compare the 18PeYuPeSu [82] EH energies to the first-principles CoYuTe levels. Fig. 3 presents a subset of the results of this comparison.

As can be seen in Fig. 3, we detect unacceptably large differences at high *K* values and the systematic, nearly horizontal differences are characterized by always the same *K* values. Thus, we decided to scrutinize the EH fits of the ground vibrational state and determine the reason behind these large discrepancies, much larger than the proven uncertainty of the first-principles CoYuTe levels (see the previous subsection).

After checking the spectroscopic database of 18PeYuPeSu [82], employed to fit a high-order Watson-type EH model to transitions corresponding to the ground vibrational state, it turned out that each high-*K* group of outliers, in fact those on the horizontal lines in Fig. 3, forms a separate FC in the experimental SN of $^{14}NH_3$. This means that although there are measured transitions connecting the energy levels within a FC of the assembled experimental SN of $^{14}NH_3$, there are no measured transitions which connect to other (high) *K* values. This in turn means that, at least in the case of $^{14}NH_3$, including transitions present in FCs in the EH fitting results in unacceptable higher-order EH parameters and energy levels even when all the transitions are fitted well. This means that

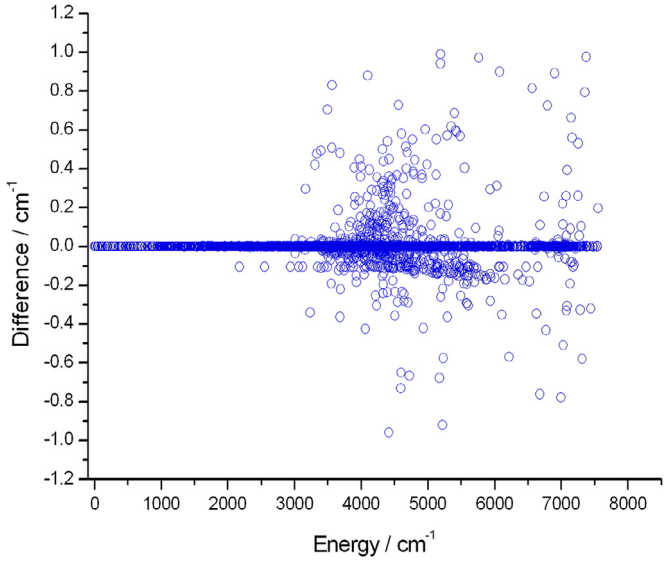

Fig. 1. Comparison of the empirical energies of $^{14}NH_3$ obtained during this study with their CoYuTe [71] counterparts.

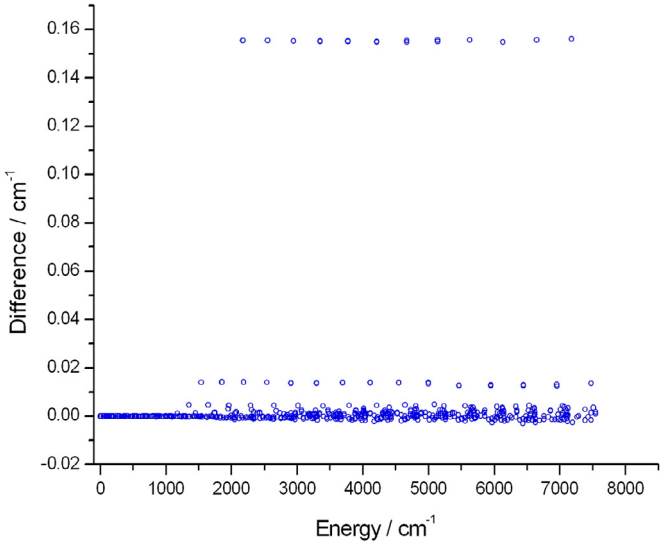

Fig. 2. Comparison of the empirical ground-vibrational-state energies of $^{14}NH_3$ of this study with their 18PeYuPeSu [82] counterparts.

Table 2
Vibrational band origins (VBO) of $^{14}NH_3$. VBO values with associated uncertainties corresponding to the last few digits are taken from the present MARVEL database, while those given in brackets correspond to first-principles estimates of Ref. [71]. See text for the meaning of the normal-mode and symmetry labels. Entries in italics correspond to "missing" vibrational energy levels of symmetry $\Gamma_{vib} = A_1'$. The number of rovibrational levels (RL) related to each vibrational parent state is given in the last column.

v_1	v_2	v_3	v_4	L_3	L_4	inv	Γ_{vib}	VBO / cm^{-1}	RL
0	0	0	0	0	0	s	A_1'	0.0(0)	351
0	0	0	0	0	0	a	A_2''	0.7934030(10)	353
0	1	0	0	0	0	s	A_1'	*[932.4]*	305
0	1	0	0	0	0	a	A_2''	968.121930(28)	309
0	2	0	0	0	0	s	A_1'	*[1597.5]*	193
0	0	0	1	0	1	s	E'	1626.27472(29)	337
0	0	0	1	0	1	a	E''	1627.37238(20)	339
0	2	0	0	0	0	a	A_2''	1882.177445(30)	230
0	3	0	0	0	0	s	A_1'	*[2384.2]*	107
0	1	0	1	0	1	s	E'	2540.5243(27)	192
0	1	0	1	0	1	a	E''	2586.12855(50)	187
0	3	0	0	0	0	a	A_2''	2895.52192(42)	101
0	2	0	1	0	1	s	E'	[3189.4]	18
0	0	0	2	0	0	s	A_1'	*[3215.9]*	58
0	0	0	2	0	0	a	A_2''	3217.57919(50)	40
0	0	0	2	0	2	s	E'	3240.16297(53)	116
0	0	0	2	0	2	a	E''	3241.59828(65)	101
1	0	0	0	0	0	s	A_1'	*[3336.1]*	61
1	0	0	0	0	0	a	A_2''	3337.09694(53)	58
0	0	1	0	1	0	s	E'	3443.62788(54)	124
0	0	1	0	1	0	a	E''	3443.98765(53)	125
0	4	0	0	0	0	s	A_1'	*[3462.4]*	45
0	2	0	1	0	1	a	E''	[3502.6]	15
0	4	0	0	0	0	a	A_2''	[4061.6]	2
0	1	0	2	0	0	s	A_1'	*[4115.9]*	4
0	1	0	2	0	2	s	E'	[4135.8]	26
0	1	0	2	0	0	a	A_2''	[4173.1]	12
0	1	0	2	0	2	a	E''	[4192.9]	22
1	1	0	0	0	0	s	A_1'	*[4294.5]*	68
1	1	0	0	0	0	a	A_2''	4320.030806(90)	68
0	1	1	0	1	0	s	E'	4416.915053(90)	111
0	1	1	0	1	0	a	E''	4435.446476(90)	103
0	2	0	2	0	2	s	E'	[4773.8]	1
0	0	0	3	0	1	s	E'	[4799.2]	2
0	0	0	3	0	1	a	E''	[4801.4]	1
0	0	0	3	0	3	s	A_1'	*[4841.6]*	1
1	0	0	1	0	1	s	E'	4955.75609(50)	98
1	0	0	1	0	1	a	E''	[4956.9]	54
1	2	0	0	0	0	s	A_1'	*[5000.2]*	3
0	0	1	1	1	1	s	A_2'	[5052.0]	7
0	0	1	1	1	1	s	E'	[5052.6]	46
0	0	1	1	1	1	a	A_1''	*[5052.7]*	6
0	0	1	1	1	1	a	E''	[5053.2]	18
0	0	1	1	1	1	a	A_2''	[5067.7]	6
0	0	1	1	1	1	s	A_1'	*[5067.8]*	9
0	2	0	2	0	0	a	A_2''	[5093.6]	6
0	4	0	1	0	1	s	E'	[5104.9]	2
0	2	1	0	1	0	s	E'	[5144.9]	14
0	2	1	0	1	0	a	E''	[5353.0]	12
0	4	0	1	0	1	a	E''	[5708.3]	1
1	1	0	1	0	1	s	E'	[5897.8]	1
1	0	0	2	0	2	s	E'	6556.4217(12)	39
1	0	0	2	0	2	a	E''	6557.9306(13)	39
1	0	0	2	0	0	s	A_1'	*[6603.8]*	1
1	0	0	2	0	0	a	A_2''	[6604.7]	1
1	0	1	0	1	0	s	E'	6608.82189(50)	75
1	0	1	0	1	0	a	E''	6609.75336(50)	73
0	0	1	2	1	2	s	A_1'	*[6650.8]*	8
0	0	1	2	1	2	a	A_1''	*[6651.7]*	6
0	0	1	2	1	2	a	A_2''	[6652.0]	2
0	0	1	2	1	2	a	E''	6678.31006(50)	64
0	0	1	2	1	2	s	E'	6677.43169(50)	66
0	2	0	3	0	1	a	E''	[6680.4]	1
0	0	2	0	0	0	a	A_2''	6795.3378(16)	29
0	0	2	0	0	0	s	A_1'	*[6796.8]*	27
0	0	2	0	2	0	s	E'	6850.2449(10)	18
0	0	2	0	2	0	a	E''	6850.6550(10)	18

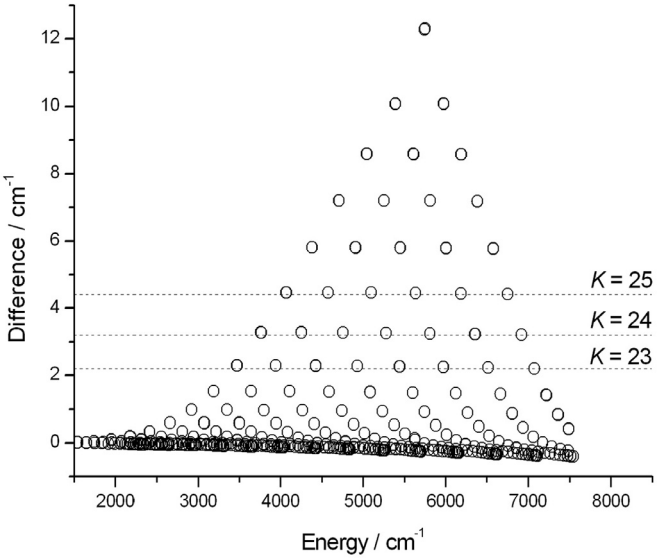

Fig. 3. Effective Hamiltonian model energies of 18PeYuPeSu [82] compared to their CoYuTe [71] first-principles counterparts above $J = 15$ on the ground vibrational state of $^{14}NH_3$.

high-K-value energy levels ($K > 18$) are ill-determined in the EH fits and as a result the corresponding energy levels derived from the sources 10YuPeDrSu [81] and 18PeYuPeSu [82] are not trustworthy. Thus, we decided to perform a new EH fit on the ground vibrational state using an extended database. The results are described in the next section.

3. New effective Hamiltonian fitting to the pure rotational transitions of $^{14}NH_3$

As mentioned in the previous section, although earlier EH fits could reproduce all the experimental transitions in the SN of $^{14}NH_3$ rather well for all vibrational parents tested, the energy values corresponding to states taking part only in FCs appear to be incorrect (see Fig. 3). Our analysis suggested that in order to obtain correct energy values we need to connect the FCs to the PCs (*ortho* and *para*) of the SN. This can be achieved, for example, by adding "artificial" transitions to the SN which connect the FCs to the two PCs. We call these transitions artificial as by design they do not need to obey any selection rules.

To check the effect of the FCs on the empirical energy levels, we created a test dataset containing only measured rotational transitions of the ground vibrational state of $^{14}NH_3$. This test dataset contains 1660 transitions, 433 of which are distributed among 47 FCs of various size. The smallest J value in the FCs is 13, while the largest one is 35. Most of the FCs consist of states of a given K value with a range of J, and there are only a few cases where the K value is less than $J/2$. The largest FC contains 62 energy levels with the associated transitions having K equal to either 13 or 16 and J in the range from 13 to 30. After employing the 10YuPeDrSu effective Hamiltonian model to these rotational test data, we obtained an EH fit (it is referred as EH Fit M hereafter, with M indicating "measurements only"). The predicted energies from Fit M exhibited basically the same behavior as depicted in Fig. 3. In other words, it became clear that the effective Hamiltonian model cannot reproduce those energy levels of CoYuTe which are part of FCs. As the next step, we decided to connect the FCs to the PCs through first-principles transitions.

By taking advantage of the proven high accuracy of the CoYuTe first-principles energies one can reliably connect the FCs to the appropriate PC. Since the test database contains 47 FCs, we would

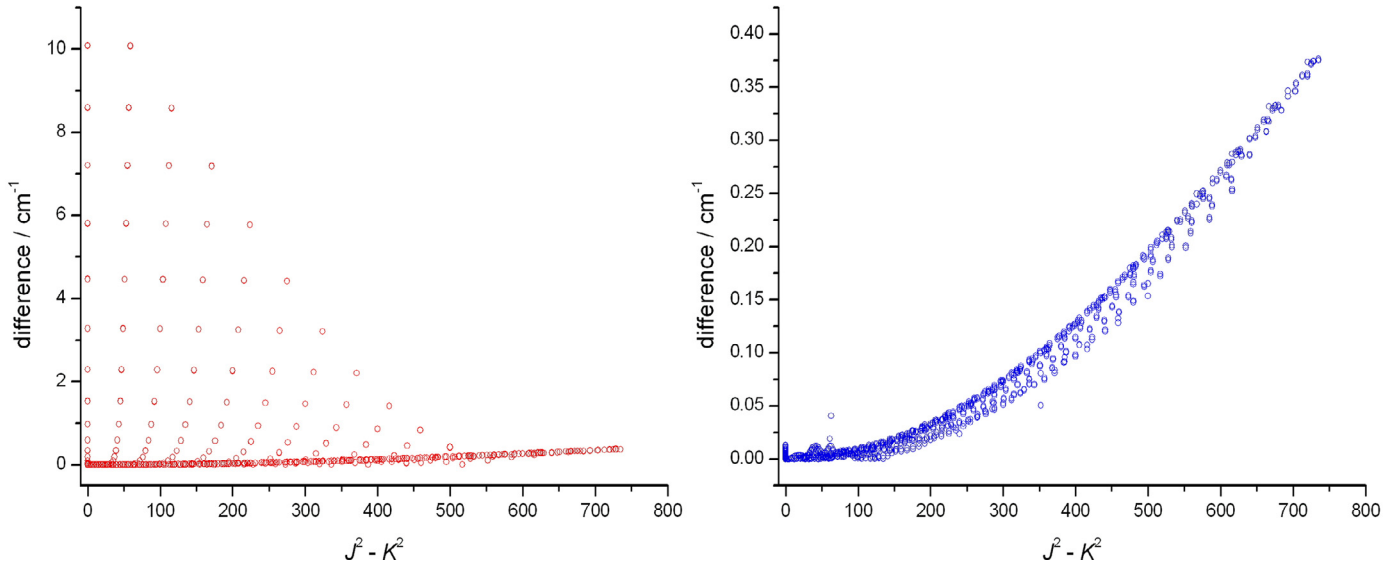

Fig. 4. Effective Hamiltonian model energies of 18PeYuPeSu [82] (left panel) and this work (right panel) compared to their CoYuTe [71] first-principles counterparts on the ground vibrational state of $^{14}NH_3$ up to 7500 cm^{-1}. Note the very different vertical scale of the two figures.

need at least 47 first-principles "artificial" transitions to eliminate all of the FCs. However, with the minimum number of connections one can not obtain an estimate of the unknown uncertainties of the theoretical lines. Therefore, we added as many computed lines to the test network as was feasible. To determine the uncertainty of a given theoretical transition we calculated the discrepancies of the cycles which contain the given first-principles transition and the absolute average of these discrepancies was accepted as the uncertainty of the first-principles "artificial" transitions. The improved test dataset thus derived for the ground vibrational state of $^{14}NH_3$ contains 1660 measured and 936 "artificial" lines. We obtained one EH fit to this improved test dataset, referred to as EH Fit A hereafter, with A indicating that "artificial" transitions have been added.

Our new Fit A can reproduce the CoYuTe energy levels almost perfectly. The left panel of Fig. 4 shows the differences between the 18PeYuPeSu [82] and the CoYuTe [71] energies, while the right panel shows the same differences using the result of Fit A based on the improved test dataset. As can be seen, each CoYuTe energy level can be reproduced by the new effective Hamiltonian model within 0.4 cm^{-1} all the way to 7500 cm^{-1}.

It is important to note that the Fit A model shows systematic deviations from the CoYuTe levels above $J = 30$. Nevertheless, since the CoYuTe energy levels were generated using the C2018 PES [41], for which the *ab initio* PES was adjusted using the experimental results only up to $J = 8$, it is hard to decide which theoretical model, the first-principles or the effective one, results in "incorrect" energy levels. Further experimental and modeling studies are needed to settle this issue.

Table 3 lists the parameters obtained from our new EH Fit A, based on all available experimental transitions as well as 936 CoYuTe first-principles energy values, our new EH Fit M, based on all available experimental transitions, and the EH fit in 10YuPeDrSu [81], based on all available experimental data in the GS (s), GS (a), ν_2 (s), and ν_2 (a), where GS refers to the ground vibrational state. The fitting input and output files are provided in the Supplementary Material, including the energy levels predicted from the new EH models. Note that Fit M was started with constants from 10YuPeDrSu [81]. Then Fit A was executed with the Fit M final constants as the initial constants, and with the CoYuTe energies with $J \geq 19$ of all K added to the fit to update the EH parameters. The Fit A parameters are updated by adding the CoYuTe energies one K at a time, and the maximum J and K values of the first-principles energies are 35. The fitting process was straightforward, and we did not experience convergence issues. Note that the 18PeYuPeSu EH model deals with higher vibrational states and its ground states' constants are fixed at those values determined from 10YuPeDrSu. Thus, the 18PeYuPeSu and 10YuPeDrSu models are exactly the same for the ground state. Here we used the 10YuPeDrSu constants as the inital constants for Fit M, because the uncertainties of the ground state constants are provided in 10YuPeDrSu but not in 18PeYuPeSu.

As shown in Table 3, the same set of 10YuPeDrSu parameters [81] is sufficient to fit the added high J and K CoYuTe energies, and additional higher-order EH parameters are not needed. When comparing EH Fit M to 10YuPeDrSu [81] (see Diff. in Column 6 of Table 3), less than 3% changes are seen in the rotational constants as well as the fourth- (D) and sixth-order (H) centrifugal-distortion constants. Up to 72% changes are seen in the eighth- and higher-order centrifugal-distortion parameters, with the exception of a 130% change in the sixteenth-order centrifugal-distortion constant P_J. Such large changes are not unexpected. NH_3 is a non-rigid molecule, and its EH model has multiple local minima when fitting to a limited set of experimental transitions that can not well constrain the model. When the experimental dataset is changed, the fitting can find another local minimum and significantly change the values of some of the EH parameters. For the levels that are experimentally observed and connected to a PC, the predicted energies from various sets of EH parameter values are expected to agree with each other; for the levels that are not experimentally observed or connected to a PC, the predicted energies may vary significantly among various sets of EH parameters. The CoYuTe first-principles energies utilized connect levels with K and J up to 35 to the PCs and constrain the EH Fit A model with the maximum number of transitions. Thus, the energies predicted from our new EH model with K and J up to 35 are not extrapolated ones.

Direct comparison of EH Fit A and EH Fit M provides useful insight into which terms might be significant and lead to discrepancies at high K values, as the difference between the two fits is only the presence of 936 CoYuTe first-principles high-K energies in Fit A. The CoYuTe first-principles energies utilized connect levels with K and J up to 35 to the PCs and constrain the Fit A model

Table 3
Spectroscopic parameters, in MHz, for the vibrational ground state of $^{14}NH_3$, where OC is Operator Code in SPFIT and SPCAT, with the last two digits denoting vibrational identifier V1V2, 00 for GS (s), 11 for GS (a), and 01 for interaction between GS (s) and GS (a) (see Ref. [81] for details). There is no well-established naming convention for the higher-order (above octic) spectroscopic constants, the one used here is the one we prefer. Diff. in Columns 4 and 6 correspond to (FitA – FitM)/FitM (FitM – 10YuPeDrSu)/10YuPeDrSu, respectively.

OC	Parameter	New fit A	Diff. (%)	New fit M	Diff. (%)	10YuPeDrSu [81]
0	E	−23785.8904(33)	0.0	−23785.8919(33)	0.0	−23785.895135(112)
100	B	298192.9106(32)	0.0	298192.9067(32)	0.0	298192.92072(104)
1000	$C-B$	−111497.0714(73)	0.0	−111497.0727(74)	0.0	−111497.0613(50)
200	$-D_J$	−25.461858(154)	0.0	−25.461567(160)	0.0	−25.461658(115)
1100	$-D_{JK}$	47.27987(56)	0.0	47.28043(58)	0.0	47.27790(62)
2000	$-D_K$	−27.35564(51)	0.0	−27.35587(59)	0.0	−27.35488(67)
300	H_J	$7.2210(74)\times10^{-3}$	0.0	$7.2226(79)\times10^{-3}$	0.5	$7.1836(90)\times10^{-3}$
1200	H_{JJK}	−0.022238(62)	−0.4	−0.022331(65)	1.5	−0.021997(80)
2100	H_{JKK}	0.023737(102)	−0.8	0.023940(107)	2.0	0.023479(133)
3000	H_K	$-8.233(48)\times10^{-3}$	−1.9	$-8.389(53)\times10^{-3}$	2.9	$-8.154(63)\times10^{-3}$
400	L_J	$-3.7693(152)\times10^{-6}$	0.5	$-3.7503(166)\times10^{-6}$	1.0	$-3.7140(141)\times10^{-6}$
1300	L_{JJK}	$1.88(34)\times10^{-6}$	−45.3	$3.44(37)\times10^{-6}$	−35.5	$5.333(279)\times10^{-6}$
2200	L_{JKK}	$0.04345(168)\times10^{-3}$	19.4	$0.03639(182)\times10^{-3}$	40.3	$0.02594(136)\times10^{-3}$
3100	L_{KKK}	$-0.07820(238)\times10^{-3}$	13.7	$-0.06875(256)\times10^{-3}$	27.4	$-0.05395(194)\times10^{-3}$
4000	LK	$0.03683(104)\times10^{-3}$	9.0	$0.03378(120)\times10^{-3}$	30.0	$0.02599(86)\times10^{-3}$
500	M_J	$2.803(38)\times10^{-9}$	3.5	$2.709(40)\times10^{-9}$	1.4	$2.671(33)\times10^{-9}$
1400	M_{JJJK}	$0.01556(61)\times10^{-6}$	21.7	$0.01279(68)\times10^{-6}$	10.7	$0.01155(49)\times10^{-6}$
2300	M_{JJKK}	$-0.1885(42)\times10^{-6}$	7.8	$-0.1748(45)\times10^{-6}$	3.2	$-0.1693(36)\times10^{-6}$
3200	M_{JKKK}	$0.4562(100)\times10^{-6}$	4.5	$0.4367(103)\times10^{-6}$	1.0	$0.4325(87)\times10^{-6}$
4100	M_{KKKK}	$-0.4214(99)\times10^{-6}$	1.9	$-0.4136(100)\times10^{-6}$	−0.7	$-0.4167(85)\times10^{-6}$
5000	M_K	$0.1347(34)\times10^{-6}$	5.1	$0.1282(41)\times10^{-6}$	−11.5	$0.14483(292)\times10^{-6}$
600	N_J	$-1.619(57)\times10^{-12}$	8.7	$-1.489(59)\times10^{-2}$	6.4	$-1.400(51)\times10^{-12}$
1500	N_{JJJK}	$-4.21(72)\times10^{-12}$	63.2	$-2.58(80)\times10^{-2}$	−9.2	$-2.84(51)\times10^{-12}$
2400	N_{JJKK}	$0.2249(72)\times10^{-9}$	11.1	$0.2025(77)\times10^{-9}$	2.2	$0.1981(57)\times10^{-9}$
3300	N_{JKKK}	$-0.8932(260)\times10^{-9}$	6.5	$-0.8390(269)\times10^{-9}$	−1.9	$-0.8555(225)\times10^{-9}$
4200	N_{JKKKK}	$1.285(41)\times10^{-9}$	0.9	$1.273(42)\times10^{-9}$	−8.4	$1.390(35)\times10^{-9}$
5100	N_{JKKKKK}	$-0.759(33)\times10^{-9}$	−6.8	$-0.814(34)\times10^{-9}$	−17.0	$-0.9811(241)\times10^{-9}$
6000	N_K	$0.1480(106)\times10^{-9}$	−24.6	$0.1964(92)\times10^{-9}$	−11.3	$0.2214(60)\times10^{-9}$
700	O_J	$0.567(43)\times10^{-15}$	19.1	$0.476(44)\times10^{-15}$	21.4	$0.392(39)\times10^{-15}$
1600	O_{JJJJK}	$-7.04(52)\times10^{-15}$	−3.8	$-7.32(55)\times10^{-15}$	−3.7	$-7.60(45)\times10^{-15}$
2500	O_{JJJKK}	$-0.1518(72)\times10^{-12}$	15.4	$-0.1315(76)\times10^{-12}$	−1.5	$-0.1335(53)\times10^{-12}$
3400	O_{JJKKK}	$0.904(41)\times10^{-12}$	4.6	$0.864(40)\times10^{-12}$	−12.9	$0.9923(257)\times10^{-12}$
4300	O_{JKKKK}	$-1.716(97)\times10^{-12}$	−4.9	$-1.805(97)\times10^{-12}$	−22.9	$-2.341(51)\times10^{-12}$
5200	O_{JKKKKK}	$1.398(109)\times10^{-12}$	−16.1	$1.666(124)\times10^{-12}$	−32.9	$2.482(48)\times10^{-12}$
6100	O_{KKKKKK}	$-0.468(57)\times10^{-12}$	−31.0	$-0.678(76)\times10^{-12}$	−43.6	$-1.2015(217)\times10^{-12}$
7000	O_K	$0.0404(105)\times10^{-12}$	−50.4	$0.0815(232)\times10^{-12}$	−68.2	$0.2561(46)\times10^{-12}$
800	P_J	$-0.0773(125)\times10^{-18}$	51.0	$-0.0512(129)\times10^{-18}$	130.6	$-0.0222(115)\times10^{-18}$
1700	P_{JJJJJK}	$2.431(165)\times10^{-18}$	−1.2	$2.461(174)\times10^{-18}$	−2.8	$2.531(162)\times10^{-18}$
2600	P_{JJJJKK}	$0.0519(33)\times10^{-15}$	13.6	$0.0457(33)\times10^{-15}$	−15.7	$0.05422(197)\times10^{-15}$
3500	P_{JJJKKK}	$-0.3612(225)\times10^{-15}$	1.3	$-0.3564(226)\times10^{-15}$	−25.0	$-0.4754(106)\times10^{-15}$
4400	$P_{JJJKKKK}$	$0.795(61)\times10^{-15}$	−8.5	$0.869(67)\times10^{-15}$	−34.0	$1.3174(244)\times10^{-15}$
5300	$P_{JJKKKKK}$	$-0.768(76)\times10^{-15}$	−18.8	$-0.946(99)\times10^{-15}$	−43.6	$-1.6766(280)\times10^{-15}$
6200	$P_{JJKKKKKK}$	$0.322(45)\times10^{-15}$	−31.0	$0.467(75)\times10^{-15}$	−55.1	$1.0391(163)\times10^{-15}$
7100	$P_{JKKKKKKK}$	$-0.0424(104)\times10^{-15}$	−46.0	$-0.0785(260)\times10^{-15}$	−72.3	$-0.2832(43)\times10^{-15}$
60000	η	$-0.1631(33)\times10^{-3}$	2.3	$-0.1595(35)\times10^{-3}$	−11.1	$-0.1794(42)\times10^{-3}$
60100	η_J	$0.17661(298)\times10^{-6}$	4.8	$0.1685(36)\times10^{-6}$	−8.9	$0.1850(38)\times10^{-6}$
61000	η_K	$-0.3805(172)\times10^{-6}$	2.1	$-0.3727(196)\times10^{-6}$	−13.3	$-0.430(32)\times10^{-6}$
111	B	298041.3739(32)	0.0	298041.3695(32)	0.0	298041.38282(104)
1011	$C-B$	−111285.5847(73)	0.0	−111285.5855(74)	0.0	−111285.5732(50)
211	$-D_J$	−24.956678(153)	0.0	−24.956360(158)	0.0	−24.956414(113)
1111	$-D_{JK}$	45.88634(55)	0.0	45.88684(57)	0.0	45.88426(61)
2011	$-D_K$	−26.40108(50)	0.0	−26.40127(58)	0.0	−26.40027(66)
311	H_J	$6.0455(71)\times10^{-3}$	0.0	$6.0463(75)\times10^{-3}$	0.6	$6.0083(86)\times10^{-3}$
1211	H_{JJK}	−0.017421(61)	−0.5	−0.017511(64)	1.9	−0.017179(78)
2111	H_{JKK}	0.017211(101)	−1.1	0.017409(106)	2.7	0.016947(131)
3011	H_K	$-5.307(47)\times10^{-3}$	−2.8	$-5.460(52)\times10^{-3}$	4.5	$-5.224(63)\times10^{-3}$
411	L_J	$-1.6434(144)\times10^{-6}$	1.6	$-1.6172(155)\times10^{-6}$	2.1	$-1.5843(127)\times10^{-6}$
1311	L_{JJK}	$-9.48(33)\times10^{-6}$	18.8	$-7.98(36)\times10^{-6}$	30.6	$-6.112(270)\times10^{-6}$
2211	L_{JKK}	$0.06616(166)\times10^{-3}$	11.7	$0.05922(180)\times10^{-3}$	21.1	$0.04890(134)\times10^{-3}$
3111	L_{KKK}	$-0.09829(236)\times10^{-3}$	10.5	$-0.08895(254)\times10^{-3}$	19.7	$-0.07428(192)\times10^{-3}$
4011	LK	$0.04347(103)\times10^{-3}$	7.5	$0.04044(119)\times10^{-3}$	23.7	$0.03269(85)\times10^{-3}$
511	M_J	$-0.241(38)\times10^{-9}$	−33.8	$-0.364(39)\times10^{-9}$	−9.5	$-0.402(33)\times10^{-9}$
1411	M_{JJJK}	$0.03489(58)\times10^{-6}$	7.7	$0.03239(64)\times10^{-6}$	3.3	$0.03135(45)\times10^{-6}$
2311	M_{JJKK}	$-0.2381(41)\times10^{-6}$	5.7	$-0.2252(43)\times10^{-6}$	2.1	$-0.2205(35)\times10^{-6}$
3211	M_{JKKK}	$0.5204(98)\times10^{-6}$	3.7	$0.5020(101)\times10^{-6}$	0.6	$0.4988(85)\times10^{-6}$
4111	M_{KKKK}	$-0.4632(97)\times10^{-6}$	1.6	$-0.4560(98)\times10^{-6}$	−0.8	$-0.4596(83)\times10^{-6}$
5011	M_K	$0.1456(34)\times10^{-6}$	4.5	$0.1393(40)\times10^{-6}$	−10.7	$0.15593(286)\times10^{-6}$
611	N_J	$1.583(57)\times10^{-12}$	−10.6	$1.771(59)\times10^{-2}$	−5.4	$1.872(52)\times10^{-12}$
1511	N_{JJJK}	$-0.02662(69)\times10^{-9}$	3.7	$-0.02566(76)\times10^{-9}$	−2.5	$-0.02633(49)\times10^{-9}$
2411	N_{JJKK}	$0.2919(69)\times10^{-9}$	7.4	$0.2719(73)\times10^{-9}$	1.0	$0.2691(53)\times10^{-9}$

(*continued on next page*)

Table 3 (*continued*)

OC	Parameter	New fit A	Diff. (%)	New fit M	Diff. (%)	10YuPeDrSu [81]
3311	N_{JJKKK}	$-1.0030(253)\times10^{-9}$	5.3	$-0.9527(261)\times10^{-9}$	−1.9	$-0.9712(214)\times10^{-9}$
4211	N_{JJKKKK}	$1.389(41)\times10^{-9}$	0.7	$1.380(41)\times10^{-9}$	−7.9	$1.498(34)\times10^{-9}$
5111	N_{JKKKKK}	$-0.812(33)\times10^{-9}$	−6.5	$-0.868(34)\times10^{-9}$	−16.2	$-1.0362(234)\times10^{-9}$
6011	N_K	$0.1596(106)\times10^{-9}$	−23.2	$0.2078(91)\times10^{-9}$	−10.9	$0.2332(59)\times10^{-9}$
711	O_J	$-1.527(43)\times10^{-15}$	−8.9	$-1.676(44)\times10^{-15}$	−5.5	$-1.773(39)\times10^{-15}$
1611	O_{JJJJJK}	$8.36(51)\times10^{-15}$	−5.1	$8.81(56)\times10^{-15}$	−0.1	$8.82(48)\times10^{-15}$
2511	O_{JJJJKK}	$-0.2018(70)\times10^{-12}$	9.4	$-0.1844(73)\times10^{-12}$	−1.5	$-0.1872(49)\times10^{-12}$
3411	O_{JJJKKK}	$1.001(41)\times10^{-12}$	3.7	$0.965(39)\times10^{-12}$	−11.7	$1.0928(242)\times10^{-12}$
4311	O_{JJKKKK}	$-1.843(97)\times10^{-12}$	−4.7	$-1.933(97)\times10^{-12}$	−21.5	$-2.463(49)\times10^{-12}$
5211	O_{JKKKKK}	$1.510(110)\times10^{-12}$	−14.8	$1.772(124)\times10^{-12}$	−31.3	$2.580(46)\times10^{-12}$
6111	O_{KKKKKK}	$-0.528(57)\times10^{-12}$	−27.9	$-0.732(76)\times10^{-12}$	−41.3	$-1.2480(211)\times10^{-12}$
7011	O_K	$0.0547(106)\times10^{-12}$	−41.8	$0.0940(230)\times10^{-12}$	−64.7	$0.2663(45)\times10^{-12}$
811	P_J	$0.5354(127)\times10^{-18}$	−8.2	$0.5830(132)\times10^{-18}$	−5.2	$0.6153(119)\times10^{-18}$
1711	P_{JJJJJK}	$-2.146(173)\times10^{-18}$	−10.8	$-2.407(187)\times10^{-18}$	0.9	$-2.385(178)\times10^{-18}$
2611	P_{JJJJKK}	$0.0671(33)\times10^{-15}$	8.2	$0.0620(33)\times10^{-15}$	−12.0	$0.07042(181)\times10^{-15}$
3511	P_{JJJKKK}	$-0.3941(228)\times10^{-15}$	0.9	$-0.3905(228)\times10^{-15}$	−23.0	$-0.5071(99)\times10^{-15}$
4411	$P_{JJJKKKK}$	$0.849(61)\times10^{-15}$	−7.8	$0.921(67)\times10^{-15}$	−32.4	$1.3620(233)\times10^{-15}$
5311	$P_{JJKKKKK}$	$-0.832(77)\times10^{-15}$	−17.0	$-1.003(99)\times10^{-15}$	−41.8	$-1.7225(271)\times10^{-15}$
6211	$P_{JJKKKKKK}$	$0.366(46)\times10^{-15}$	−27.5	$0.505(75)\times10^{-15}$	−52.7	$1.0683(160)\times10^{-15}$
7111	$P_{JKKKKKKK}$	$-0.0552(105)\times10^{-15}$	−38.5	$-0.0897(258)\times10^{-15}$	−69.2	$-0.2914(42)\times10^{-15}$
60,011	η	$-0.1628(34)\times10^{-3}$	2.3	$-0.1592(36)\times10^{-3}$	−11.4	$-0.1797(43)\times10^{-3}$
60,111	η_J	$0.17669(305)\times10^{-6}$	4.9	$0.1685(37)\times10^{-6}$	−9.3	$0.1857(39)\times10^{-6}$
61,011	η_K	$-0.4198(163)\times10^{-6}$	1.6	$-0.4133(187)\times10^{-6}$	−8.8	$-0.4533(315)\times10^{-6}$
230001	α	−8.650(45)	0.4	−8.614(48)	−3.2	−8.896(54)
230101	α_J	$5.6508(299)\times10^{-3}$	1.5	$5.566(40)\times10^{-3}$	−2.6	$5.716(38)\times10^{-3}$
230201	α_{JJ}	$-1.7587(73)\times10^{-6}$	1.8	$-1.7276(119)\times10^{-6}$	2.9	$-1.6791(112)\times10^{-6}$
230301	α_{JJJ}	$1.0305(132)\times10^{-9}$	7.7	$0.9566(209)\times10^{-9}$	0.1	$0.9558(157)\times10^{-9}$
231001	α_K	−0.03343(75)	9.0	−0.03066(81)	20.9	−0.02536(54)
231101	α_{JK}	$0.06667(94)\times10^{-3}$	6.8	$0.06245(107)\times10^{-3}$	3.4	$0.06039(76)\times10^{-3}$
231201	α_{JJK}	$-0.02862(52)\times10^{-6}$	4.8	$-0.02731(62)\times10^{-6}$	−6.2	$-0.029115(303)\times10^{-6}$
232101	α_{JKK}	$0.03176(131)\times10^{-6}$	−12.0	$0.03608(168)\times10^{-6}$	−27.6	$0.04986(32)\times10^{-6}$
232001	α_{KK}	$-0.03217(149)\times10^{-3}$	−18.3	$-0.03936(177)\times10^{-3}$	−25.1	$-0.05257(45)\times10^{-3}$
233001	α_{KKK}	$-1.51(44)\times10^{-9}$	−37.1	$-2.40(97)\times10^{-9}$	−69.5	$-7.858(89)\times10^{-9}$

with a large number of transitions. Thus, we expect improved uncertainties for the terms leading to the discrepancies at high K. In fact, the parameters O_K and $P_{JKKKKKKK}$ have the most reduced uncertainties, with uncertainty values in EH Fit A being ∼40% and ∼45% of those in Fit M. In addition, the following terms are determined with significantly reduced uncertainties: $P_{JJKKKKKK}$(∼60%), $P_{JJJKKKKK}$(∼75%), and $O_{JJKKKKK}$ (∼75%). The rest of the centrifugal-distortion constants changed by less than 10%. Our conclusion is that the constants mentioned play the most significant role in the discrepancies observed at high K values.

A referee of this paper called our attention to a study of Costain [74]. Costain fitted microwave ammonia transitions using the empirical formula

$$\nu = \nu_0 \exp[AJ(J+1) + BK^2 + CJ^2(J+1)^2 + DJ(J+1)K^2 + EK^4] \quad (1)$$

and suggested that the inversion spectrum might be more accurately represented by this formula than by the usual expression used in this work and 10YuPeDrSu [81]. Table S1 of the Supplementary Material lists the lines fitted by Costain [74], the fitting residuals obtained by Costain [74] and those characterizing our EH models. The comparison of fitting residuals indicates that the lines available to Costain are represented better by our EH models. This may be due to the fact that we include many more high J and K lines in our EH models than the 64 lines Costain [74] dealt with. Nevertheless, in a future work we plan to incorporate this empirical formula to fit the data included in EH Fit A and establish the performance of this model.

4. Highly accurate rotational lines of $^{14}NH_3$

A common feature of most present-day line-by-line spectroscopic databases, including HITRAN 2016 [158], is that they are based almost exclusively on lines obtained from Doppler-broadened spectra. The usual Doppler linewidth is about 1–5 GHz, strongly limiting the accuracy of the high-resolution lines measured and the resolution of the experiments. Modern laser-spectroscopy measurements, based on frequency combs, cavity enhancement, saturation, and other recent experimental advances, allow Doppler-free measurement of certain lines. The accuracy of these measurements approach the 1 kHz region [106], though in principle it can be even better.

Several scientific and engineering applications need the protection of certain narrow regions around lines so that observations of these molecular transitions, perhaps of astronomical interest, will not be hindered by man-made activities. Due to an effort of a number of international organizations over several decades, a number of lines with frequencies less than 3 THz for a number of molecules, including ammonia, have become protected [159]. The $^{14}NH_3$ lines under protection by certain international bodies associated with the National Academies of Sciences, Engineering, and Medicine (NASEM) [159] are listed in Table 4.

As shown in Table 4, our MARVEL database contains several sources reporting measurements of the lines protected with an accuracy down to 0.2 kHz. The present MARVEL analysis of all available high-resolution spectroscopic information for $^{14}NH_3$ confirms the accuracy of the best measurements. Furthermore, in a few cases MARVEL even improves upon the accuracy of the best measurements. In fact, above 2 THz there are several lines, given in Table 4 as boldface entries under f(MARVEL), where the empirical estimates of the present study have tighter uncertainties than the best measurements. Fig. 5 illustrates two such cases. Finally, we note that the designation of quite a few lines above 1 THz used by NASEM [159] are incorrect by more than 2 MHz. These entries are italicized in the first column of Table 4. There are three cases, the lines at 2405.121, 2991.555, and 2994.786 GHz, where both the NASEM designations are incorrect and we obtain higher accuracy as a result of our MARVEL analysis than the best measure-

Table 4
Rotational lines of $^{14}NH_3$ under protection by international bodies associated with the National Academies of Sciences, Engineering, and Medicine (NASEM) [159] and their various experimental and empirical determinations. All values are in GHz and all lines belong to the vibrational ground state. For each line all measurements treated during the MARVEL analysis are reported. A NASEM entry in italics indicates that the difference between MARVEL and NASEM is larger than 2 MHz. Boldface MARVEL entries correspond to empirical predictions more accurate than the most precise direct measurements.

f(NASEM)/GHz	$J'\ K'\ inv' \leftarrow J''\ K''\ inv''$	*f*(MARVEL)/GHz	*f*(expt)/GHz
23.694	$1\,1\,a \leftarrow 1\,1\,s$	23.694 495 49(21)	23.694 495 49(21) [43]
			23.694 496 0(50) [110]
23.723	$2\,2\,a \leftarrow 2\,2\,s$	23.722 633 32(21)	23.722 633 32(21) [43]
			23.722 631 0(50) [110]
23.870	$3\,3\,a \leftarrow 3\,3\,s$	23.870 129 17(21)	23.870 129 17(21) [43]
			23.870 130 0(50) [110]
572.498	$1\,0\,s \leftarrow 0\,0\,a$	572.498 159 87(24)	572.498 159 93(18) [64]
			572.498 159 78(21) [64]
			572.498 1(24) [54]
			572.498 1(30) [128]
1168.452	$2\,1\,s \leftarrow 1\,1\,a$	1168.452 397(23)	1168.452 394(20) [62]
			1168.452 413(51) [81]
			1168.451 6(24) [54]
			1168.477(26) [128]
			1168.480(29) [139]
1214.859	$2\,0\,a \leftarrow 1\,0\,s$	1214.852 942(20)	1214.852 942(20) [62]
			1214.852 87(14) [116]
			1214.858 6(59) [54]
			1214.846(18) [139]
1215.245	$2\,1\,a \leftarrow 1\,1\,s$	1215.245 711(23)	1215.245 714(20) [62]
			1215.245 67(18) [116]
			1215.245 3(24) [54]
			1215.272(27) [139]
1763.525	$3\,0\,s \leftarrow 2\,0\,a$	1763.524 359(99)	1763.524 358(99) [81]
			1763.525 2(24) [54]
			1763.544(21) [139]
1763.602	$3\,1\,s \leftarrow 2\,1\,a$	**1763.601 227(81)**	1763.601 219(99) [81]
			1763.602 0(24) [54]
1763.821	$3\,2\,s \leftarrow 2\,2\,a$	1763.823 18(13)	1763.823 186(99) [81]
			1763.821 4(24) [54]
			1763.778(47) [139]
1808.936	$3\,1\,a \leftarrow 2\,1\,s$	**1808.934 551(81)**	1808.934 564(99) [81]
			1808.935 4(24) [54]
			1808.936(18) [139]
			1808.969(36) [128]
1810.378	$3\,2\,a \leftarrow 2\,2\,s$	1810.380 00(13)	1810.379 971(99) [81]
			1810.377 7(24) [54]
			1810.369(18) [139]
			1810.357(24) [128]
2357.210	$4\,1\,s \leftarrow 3\,1\,a$	2357.209 99(10)	2357.209 920(99) [81]
			2357.210 2(24) [54]
			2357.199(18) [139]
2357.727	$4\,2\,s \leftarrow 3\,2\,a$	2357.728 46(13)	2357.728 417(99) [81]
			2357.726 8(24) [54]
			2357.697(33) [139]
2358.563	$4\,3\,s \leftarrow 3\,3\,a$	2358.566 19(17)	2358.566 118(99) [81]
			2358.563 2(31) [54]
			2358.551(18) [139]
2400.018	$4\,0\,a \leftarrow 3\,0\,s$	2400.020 831(99)	2400.020 831(99) [81]
			2400.017 6(34) [54]
			2400.024(18) [139]
2400.578	$4\,1\,a \leftarrow 3\,1\,s$	**2400.578 800(78)**	2400.578 775(99) [81]
			2400.578 5(24) [54]
			2400.573(18) [139]
2402.265	$4\,2\,a \leftarrow 3\,2\,s$	2402.266 00(13)	2402.266 037(99) [81]
			2402.264 8(24) [54]
			2402.252(18) [139]
2405.121	$4\,3\,a \leftarrow 3\,3\,s$	**2405.124 63(17)**	2405.121 3(35) [54]
			2405.118(18) [139]
2948.411	$5\,0\,s \leftarrow 4\,0\,a$	2948.395 32(14)	2948.395 304(99) [81]
			2948.411(16) [54]
			2948.375(21) [139]
2948.669	$5\,1\,s \leftarrow 4\,1\,a$	2948.668 64(13)	2948.668 655(99) [81]
			2948.669 3(24) [54]
			2948.711(44) [139]
2949.480	$5\,2\,s \leftarrow 4\,2\,a$	2949.482 41(16)	2949.482 400(99) [81]
			2949.480 5(24) [54]
			2949.457(27) [139]

(*continued on next page*)

Table 4 (*continued*)

f(NASEM)/GHz	$J'\ K'\ in\nu' \leftarrow J''\ K''\ in\nu''$	*f*(MARVEL)/GHz	*f*(expt)/GHz
2950.815	5 3 *s* ← 4 3 *a*	2950.819 80(13)	2950.819 774(99) [81]
			2950.814 6(54) [54]
			2950.800(21) [139]
2952.640	5 4 *s* ← 4 4 *a*	2952.638 37(10)	2952.638 366(99) [81]
			2952.639 7(24) [54]
			2952.632(18) [139]
2989.643	5 1 *a* ← 4 1 *s*	**2989.641 29(12)**	2989.642 5(24) [54]
			2989.641 3(30) [128]
			2989.632(18) [139]
2991.555	5 2 *a* ← 4 2 *s*	**2991.557 32(16)**	2991.555 2(24) [54]
			2991.533(26) [139]
			2991.527(32) [128]
2994.786	5 3 *a* ← 4 3 *s*	**2994.793 39(13)**	2994.786 4(73) [54]
			2994.780(18) [139]
			2994.822(30) [128]
2999.430	5 4 *a* ← 4 4 *s*	**2999.430 81(10)**	2999.430 1(24) [54]
			2999.418(14) [128]
			2999.400(33) [139]

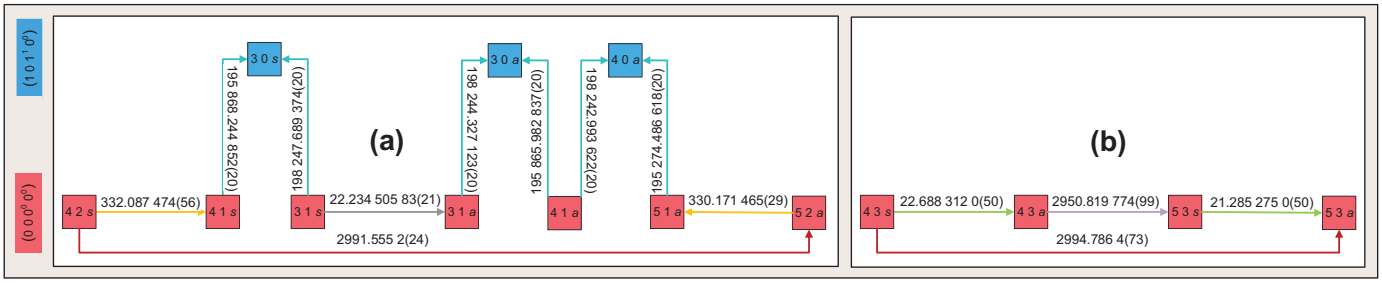

Fig. 5. Highly accurate frequency determinations for lines at 2991.555 [panel (a)] and 2994.786 GHz [panel (b)] NASEM frequencies (see also Table 4). The *J K inν* rotational labels within the squares represent rovibrational states, whose $(\nu_1\nu_2^{l_2}\nu_3^{l_3}\nu_4^{l_4})$ vibrational labels are indicated in the left-hand-side legend with different colors. Transitions designated with orange, cyan, gray, brown, green, and purple arrows are results from 88TaEnHi [111], 16TwHaSe [30], 70KuWo [44], 83PoMa [54], 75PoKa [110], and 10YuPeDrSu [81], respectively. Lines are augmented with their experimental frequencies (in GHz) and the uncertainties of the last few frequency digits given in parentheses. In both cases (a) and (b), the brown connectors of 83PoMa denote the best available observations for the corresponding transitions. Employing the Ritz principle successively, the following empirical predictions are derived from the two underlying network paths: 332.087 474 + 195 868.244 852 − 198 247.689 374 + 22.234 505 83 + 198 244.327 123 − 195 865.982 837 + 198 242.993 622 − 195 274.486 618 − 330.171 465 ≈ 2991.557 284 and 22.688 312 0 + 2950.819 774 + 21.285 275 0 ≈ 2994.793 361 GHz. These two estimates can be associated with the uncertainties of $\sqrt{56^2+20^2+20^2+0.21^2+20^2+20^2+20^2+20^2+29^2} \approx 80$ and $\sqrt{5^2+99^2+5^2} \approx 99$ kHz, respectively. These path-based frequencies, together with the MARVEL-predicted values utilizing the full network information [2991.557 31(11) and 2994.793 39(13) GHz, see Table 4], are at least 10 times more accurate than the direct brown links of 83PoMa [54]. (For interpretation of the references to color in this figure legend, the reader is referred to the web version of this article.)

ments. The correct designations of these lines would be 2405.125, 2991.557, and 2994.793 GHz, respectively. The origin of the incorrect designations can be found in the last column of Table 4. It would be interesting to see if new, ultraprecise measurements confirmed the proposed empirical line positions of this study (see also Fig. 5).

5. Conclusions

One of the aims of the present study has been a comprehensive revision and extension of previous MARVEL analyses [13,22] of the measured rovibrational transitions and energy levels of $^{14}NH_3$. A significant restriction, making the present study drastically different from all previous MARVEL investigations, is that only those transitions were considered here which involve states with energies less than 7500 cm^{-1} and our study is also constrained to the PCs of the experimental SN of $^{14}NH_3$. The most notable characteristics and results of the present investigation can be summarized as follows:

(1) The final empirical energy list contains 4936 uniquely labelled states below 7500 cm^{-1}. In a previous similar study [22] the number of empirical energy levels below 7500 cm^{-1} was 4716. These two numbers should be compared to about 26 500, the number of rovibrational energy levels first-principles computations suggest below the energy cutoff of 7500 cm^{-1}.

(2) While we treated significantly (65%) more transitions and involved 28 new sources during this investigation, compared to Al-Derzi et al. [22], the number of energy levels increased only marginally, by 5%. This points toward the need of an improved design of high-resolution spectroscopic measurements to significantly increase the utility of new data.

(3) The rovibrational measurements covered in this study involve all possible vibrational bands only up to 4000 cm^{-1}, the first vibrational band missing is at 4008 cm^{-1}. Furthermore, about half of the vibrational states are missing between 4000 and 6000 cm^{-1}. The situation deteriorates quickly above 6000 cm^{-1}. To remedy this problem requires careful experimental studies of the region above 4000 cm^{-1}, which should be helped considerably by the results presented here.

(4) The empirical rovibrational levels of $^{14}NH_3$ form a complete set up to 2412.7 cm^{-1}.

In the second part of our study we have identified problems with previous effective Hamiltonian fits associated with floating components leading to correctly fitted transition frequencies but erroneous energy levels. We were able to cure this problem by the judicious use of computed transitions which link the various floating components with the principal components. This issue is a general one for systems which have restrictive selection or propensity rules, such as the dominant $\Delta K = 0$ rule in ammonia. Our procedure, combining network theory and first-principles compu-

tations, offers a way forward in such situations. In fact, using a Watson Hamiltonian with terms up to sixteenth order and utilizing carefully chosen and well-characterized artificial transitions taken from the CoYuTe line list [71] we were able to generate new effective-Hamiltonian parameters for the ground vibrational state of $^{14}NH_3$, which predict correct energy levels for this state for levels with $K \leq 25$. This effort was, in part, undertaken to address an impasse in the intercomparison of experimental and theoretical energy levels for ammonia. In addition to improving the ability of the effective Hamiltonian to predict energy levels, the method developed here enables the synergetic trust of MARVEL levels that can reliably compare to computed linelists.

Comparisons with our empirical energies help to validate the accuracy of the C2018 PES [70] which underpins the CoYuTe line list. Notwithstanding this comment, the variational nuclear motion calculations used to generate the CoYuTe line list do not produce energy levels with the same accuracy as the MARVEL procedure utilized here. While all the analyses presented in this work which used CoYuTe data used the original computed energy levels, the final CoYuTe line list actually replaced these levels with the MARVEL ones from this work where available [71]. Besides the obvious advantages in terms of improved frequencies, there are a number of specific reasons for doing this. The ExoMol project [72,73], for which CoYuTe was created, aims to produce comprehensive line lists for the characterization of exoplanetary atmospheres. Recently, Doppler-shift high-resolution spectroscopy has been found to be a powerful way of detecting molecules on exoplanets [160]. This technique requires high experimental accuracy for the line positions. Similarly, the most recent HITRAN database [158] is missing a significant number of lines in the 4000 – 7000 cm^{-1} region. The "BARVEL" line list [38] constructed using the previous MARVEL energy levels and the BYTe line list [67] was found to be insufficiently accurate for this purpose [158]; hopefully a line list constructed using the improved CoYuTe intensities and the updated MARVEL energy levels will prove to be more reliable.

Our study confirms the accuracy of a number of measured lines relevant for the efforts of international organizations protecting certain $^{14}NH_3$ lines under 3 THz [159]. Furthermore, in a few cases we suggest significantly more accurate frequencies for some of the lines, supported by the spectroscopic network of the measured lines.

Finally, the present study was restricted to transition wavenumbers below 7500 cm^{-1} (note that the restriction applied was on the energy levels but this is a direct consequence of our choice). However, ammonia spectra are important at shorter wavelengths than this. For example, visible spectra of ammonia are well known in Jupiter [161]. Recent work has shown that the CoYuTe line list gives the best available model for this spectrum but that there is a significant shift in the line positions [162]. A MARVEL-based study covering these wavelengths would rectify these problems but would require further laboratory high-resolution spectra recorded at near infrared and visible wavelengths first.

Declaration of Competing Interest

The authors declare that they have no known competing financial interests or personal relationships that could have appeared to influence the work reported in this paper.

CRediT authorship contribution statement

Tibor Furtenbacher: Methodology, Software, Investigation, Validation, Formal analysis. **Phillip A. Coles:** Data curation, Investigation, Writing - original draft, Writing - review & editing. **Jonathan Tennyson:** Investigation, Supervision, Writing - review & editing, Funding acquisition. **Sergei N. Yurchenko:** Supervision. **Shanshan Yu:** Software, Validation, Writing - original draft, Writing - review & editing, Formal analysis. **Brian Drouin:** Validation, Writing - original draft, Writing - review & editing, Funding acquisition. **Roland Tóbiás:** Methodology, Software, Investigation, Visualization, Formal analysis. **Attila G. Császár:** Conceptualization, Supervision, Writing - review & editing, Funding acquisition.

Acknowledgements

The Hungarian co-authors are grateful to NKFIH (grant no. K119658) and the framework of the ELTE Excellence Program (1783-3/2018/FEKUTSTRAT) supported by the Hungarian Ministry of Human Capacities (EMMI) for generous support. PAC thanks EPSRC for a CASE studentship under grant EP/L504889/1 and Servomex for industrial sponsorship. SY and JT thank STFC for grant ST/M001334/1. Collaborative work between the ELTE and UCL teams received support from the COST action CM1405, MOLIM: Molecules in Motion. Part of the research described in this paper was carried out at the Jet Propulsion Laboratory, California Institute of Technology, under a contract with the National Aeronautics and Space Administration (80NM0018D0004). The authors are grateful to Dr. Jan Smydke for his comments on the labels of the vibrational states of $^{14}NH_3$ and to Prof. Trevor Sears for useful discussions about some of the data of Ref. [30].

Supplementary material

Supplementary material associated with this article can be found, in the online version, at doi:10.1016/j.jqsrt.2020.107027.

References

[1] Galloway JN, Aber JD, Erisman JW, Seitzinger SP, Howarth RW, Cowling EB, et al. The nitrogen cascade. Bioscience 2003;53:341–56.
[2] Erisman JW, Galloway JN, Seitzinger S, Bleeker A, Dise NB, Petrescu AMR, et al. Consequences of human modification of the global nitrogen cycle. Phil Trans R Soc Lond B 2013;368:20130116.
[3] Van Damme M, Clarisse L, Whitburn S, Hadji-Lazaro J, Hurtmans D, Clerbaux C, et al. Industrial and agricultural ammonia point sources exposed. Nature 2018;564:99–103.
[4] Cheung A, Rank DM, Townes CH, Thornton DD, Welch WJ. Detection of NH_3 molecules in the interstellar medium by their microwave emission. Phys Rev Lett 1968;21:1701–5.
[5] Cheung AC, Rank DM, Townes CH, Thornton DD, Welch WJ. Detection of water in interstellar regions by its microwave radiation. Nature 1969;221:626–8.
[6] Ho PTP, Townes CH. Interstellar ammonia. Ann Rev Astron Astrophys 1983;21:239–70.
[7] MacDonald RJ, Madhusudhan N. HD 209458b in new light: evidence of nitrogen chemistry, patchy clouds and sub-solar water. Mon Not R Astron Soc 2017;469:1979–96.
[8] Lucas PW, Tinney CG, Burningham B, Leggett SK, Pinfield DJ, Smart R, et al. The discovery of a very cool, very nearby brown dwarf in the Galactic plane. Mon Not R Astron Soc 2010;408:L56–60.
[9] Schneider AC, Cushing MC, Kirkpatrick JD, Gelino CR, Mace GN, Wright EL, et al. Hubble space telescope spectroscopy of brown dwarfs discovered with the wide-field infrared survey explorer. Astrophys J 2015;804:92.
[10] Canty JI, Lucas PW, Tennyson J, Yurchenko SN, Leggett SK, Tinney CG, et al. Methane and ammonia in the near-infrared spectra of late-T dwarfs. Mon Not R Astron Soc 2015;450:454–80.
[11] Cleeton CE, Williams NH. Electromagnetic waves of 1.1 cm wave-length and the absorption spectrum of ammonia. Phys Rev 1934;45:234–7.
[12] Klopper W, Samson CCM, Tarczay G, Császár AG. Equilibrium inversion barrier of NH_3 from extrapolated coupled-cluster pair energies. J Comp Chem 2001;22:1306–14.
[13] Császár AG, Furtenbacher T. Promoting and inhibiting tunneling via nuclear motions. Phys Chem Chem Phys 2016;18:1092–104.
[14] Fábri C, Marquardt R, Császár AG, Quack M. Controlling tunneling in ammonia isotopomers. J Chem Phys 2019;150:014102.
[15] Markov N. A quantum propulsion method. In: Georgiev P, Soares CG, editors. Sustainable development and innovations in marine technologies; vol. 3 of proceedings in marine technology and ocean engineering. Maritime Assoc Mediterranean; Tech Univ Varna; 2020. p. 247–51. ISBN 978-0-367-81008-5; 978-0-367-40951-7 18th International Congress of the Maritime-Association-of-the-Mediterreanean (IMAM), Varna, BULGARIA, SEP 09–11, 2019.
[16] Lemarchand C, Triki M, Darquie B, Borde CJ, Chardonnet C, Daussy C. Progress towards an accurate determination of the Boltzmann constant by Doppler spectroscopy. New J Phys 2011;13:073028.

[17] Triki M, Lemarchand C, Darquie B, Sow PLT, Roncin V, Chardonnet C, et al. Speed-dependent effects in NH_3 self-broadened spectra: towards the determination of the Boltzmann constant. Phys Rev A 2012;85:062510.

[18] Lemarchand C, Mejri S, Sow PLT, Triki M, Tokunaga SK, Briaudeau S, et al. A revised uncertainty budget for measuring the Boltzmann constant using the Doppler broadening technique on ammonia. Metrologica 2013;50:623–30.

[19] Bethlem HL, Kajita M, Sartakov B, Meijer G, Ubachs W. Prospects for precision measurements on ammonia molecules in a fountain. Eur Phys J D 2008;163:55–69.

[20] Owens A, Yurchenko SN, Thiel W, Špirko V. Accurate prediction of the ammonia probes of a variable proton-to-electron mass ratio. Mon Not R Astron Soc 2015;450:3191–200.

[21] Owens A, Yurchenko SN, Thiel W, Spirko V. Enhanced sensitivity to a possible variation of the proton-to-electron mass ratio in ammonia. Phys Rev A 2016;93:052506.

[22] Al Derzi AR, Furtenbacher T, Yurchenko SN, Tennyson J, Császár AG. MARVEL analysis of the measured high-resolution spectra of $^{14}NH_3$. J Quant Spectrosc Radiat Transf 2015;161:117–30.

[23] Furtenbacher T, Császár AG, Tennyson J. MARVEL: Measured active rotational-vibrational energy levels. J Mol Spectrosc 2007;245:115–25.

[24] Furtenbacher T, Császár AG. MARVEL: measured active rotational-vibrational energy levels. II. Algorithmic improvements. J Quant Spectrosc Radiat Transf 2012;113:929–35.

[25] Tóbiás R, Furtenbacher T, Tennyson J, Császár AG. Accurate empirical rovibrational energies and transitions of $H_2{}^{16}O$. Phys Chem Chem Phys 2019;21:3473–95.

[26] Császár AG, Furtenbacher T. Spectroscopic networks. J Mol Spectrosc 2011;266:99–103.

[27] Furtenbacher T, Császár AG. The role of intensities in determining characteristics of spectroscopic networks. J Molec Struct (THEOCHEM) 2012;1009:123–9.

[28] Császár AG, Furtenbacher T, Árendás P. Small molecules – big data. J Phys Chem A 2016;120:8949–69.

[29] Yachmenev A, Kuepper J. Communication: General variational approach to nuclear-quadrupole coupling in rovibrational spectra of polyatomic molecules. J Chem Phys 2017;147:141101.

[30] Twagirayezu S, Hall GE, Sears TJ. Quadrupole splittings in the near-infrared spectrum of $^{14}NH_3$. J Chem Phys 2016;145:144302.

[31] Aroui H, BenMabrouk K, Boussassi R. Line-mixing effect on NH_3 line intensities. J Quant Spectrosc Radiat Transf 2013;130:273–83.

[32] JBarton E, Yurchenko SN, Tennyson J, Clausen S, Fateev A. High-resolution absorption measurements of NH_3 at high temperatures: 500–2100 cm^{-1}. J Quant Spectrosc Radiat Transf 2015;167:126–34.

[33] Pearson JC, Yu S, Pirali O. Modeling the spectrum of the $2\nu_2$ and ν_4 states of ammonia to experimental accuracy. J Chem Phys 2016;145:124301.

[34] Sung K, Yu S, Pearson J, Pirali O, Tchana FK, Manceron L. Far-infrared $^{14}NH_3$ line positions and intensities measured with a FT-IR and AILES beamline, synchrotron SOLEIL. J Mol Spectrosc 2016;327:1–20.

[35] Barton EJ, Yurchenko SN, Tennyson J, Béguier S, Campargue A. A near infrared line list for NH_3: analysis of a Kitt Peak spectrum after 35 years. J Mol Spectrosc 2016;325:7–12.

[36] Fusina L, Di Lonardo G, Cane E, Predoi-Cross A, Rozario H, Herman M. The high resolution spectrum of $^{15}NH_3$ in the far-infrared: rotation-inversion transitions in the ground, $\nu_2 = 1, 2$ and $\nu_4 = 1$ states. J Quant Spectrosc Radiat Transf 2017;203:417–24.

[37] Barton EJ, Yurchenko SN, Tennyson J, Clausen S, Fateev A. High-resolution absorption measurements of NH_3 at high temperatures: 2100 - 5500 cm^{-1}. J Quant Spectrosc Radiat Transf 2017;189:60–5.

[38] Beale CA, Hargreaves RJ, Coles P, Tennyson J, Bernath PF. Infrared absorption spectra of hot ammonia. J Quant Spectrosc Radiat Transf 2017;203:410–16.

[39] Barton EJ, Polyansky OL, Yurchenko SN, Tennyson J, Civis S, Ferus M, et al. Absorption spectra of ammonia near 1 µm. J Quant Spectrosc Radiat Transf 2017;203:392–7.

[40] Zobov NF, Coles PA, Ovsyannikov RI, Kyuberis AA, Hargreaves RJ, Bernath PF, et al. Analysis of the red and green optical absorption spectrum of gas phase ammonia. J Quant Spectrosc Radiat Transf 2018;209:224–31.

[41] Coles PA, Ovsyannikov RI, Polyansky OL, Yurchenko SN, Tennyson J. Improved potential energy surface and spectral assignments for ammonia in the near-infrared region. J Quant Spectrosc Radiat Transf 2018;219:199–212.

[42] Kukolich SG. Measurement of hyperfine structure of the $J = 3$, $K = 2$ inversion line of $^{14}NH_3$. Phys Rev 1965;138(5A):A1322–5.

[43] Kukolich SG. Measurement of ammonia hyperfine structure with a two-cavity maser. Phys Rev 1967;156:83–92.

[44] Kukolich SG, Wofsy SC. $^{14}NH_3$ hyperfine structure and quadrupole coupling. J Chem Phys 1970;52:5477–81.

[45] Freund SM, Oka T. Infrared-microwave two-photon spectroscopy: the ν_2 band of NH_3. Phys Rev A 1976;13:2178–90.

[46] Hillman JJ, Kostiuk T, Buhl D, Faris JL, Novaco JC, Mumma MJ. Precision measurements of NH_3 spectral lines near 11 µm using the infrared heterodyne technique. Opt Lett 1977;1(3):81.

[47] Kostiuk T, Mumma MJ, Hillman JJ, Buhl D, Brown LW, Faris JL. NH_3 spectral line measurements on Earth and Jupiter using 10 mm superheterodyne receiver. Infrared Phys 1977;17:431–9.

[48] Jones H. Infrared-microwave two-photon spectroscopy with $^{13}C^{16}O_2$ and $^{12}C^{18}O_2$ lasers of the ν_2-band of ammonia. Appl Phys 1978;15(3):261–4.

[49] Belov SP, Gershstein LI, Krupnov AF, Maslovskij AV, Urban Š, Špirko V, et al. Inversion and inversion-rotation spectrum of $^{14}NH_3$ in the ν_2 excited state. J Mol Spectrosc 1980;84:288–304.

[50] Sinha BV, Smith PDP. New microwave inversion lines of $^{14}NH_3$ in the ground state. J Mol Spectrosc 1980;80:231–2.

[51] Sattler JP, Worchesky TL. Additional diode laser heterodyne measurements on ammonia. J Mol Spectrosc 1981;90:297–301.

[52] Minguzzi P, Tonelli M, Carrozzi A, Lieto AD. Optoacoustic laser Stark spectroscopy in the ν_2 band of $^{14}NH_3$. J Mol Spectrosc 1982;96(2):294–305.

[53] Shoja-Chaghervand P, Bjarnov E, Schwendeman R. Infrared-microwave two-photon spectroscopy of the ν_2 band of $^{14}NH_3$. J Mol Spectrosc 1983;97(2):287–305.

[54] Poynter RL, Margolis JS. The ground state far infrared spectrum of NH_3. Mol Phys 1983;48:401–18.

[55] Magerl G, Schupita W, Frye JM, Kreiner WA, Oka T. Sub-doppler spectroscopy of the ν_2 band of NH_3 using microwave modulation sidebands of CO_2 laser lines. J Mol Spectrosc 1984;107(1):72–83.

[56] Siemsen KJ, Reid J. Heterodyne frequency measurements of $^{14}NH_3$ and $^{15}NH_3\nu_2$-band transitions. Optics Lett 1985;10:594–6.

[57] D'Cunha R. The $a2\nu_2 \leftarrow s\nu_2$ bands of $^{14}NH_3$ and $^{15}NH_3$. J Mol Spectrosc 1987;122:130–4.

[58] Lellouch E, Lacome N, Guelachvili G, Tarrago G, Encrenaz T. Ammonia: experimental absolute linestrengths and self-broadening parameters in the 1800 to 2100 cm^{-1} range. J Mol Spectrosc 1987;124:333–47.

[59] Snels M, Baldacchini G. Shape and width of IR absorption lines of ammonia expanded in a supersonic jet. Appl Phys B 1988;47:277–82.

[60] Smith PDP, Firth S, Davis RW. High J inversion lines of ammonia. J Mol Spectrosc 1990;144:448–50.

[61] Fabian M, Ito F, Yamada KMT. N_2, O_2, and air broadening of NH_3 in ν_2 band measured by FTIR spectroscopy. J Mol Spectrosc 1995;173:591–602.

[62] Winnewisser G, Belov SP, Klaus T, Urban S. Ro-inversional spectrum of ammonia. Z Naturforsch 1996;51:200–6.

[63] Sun Z-D, Lees RM, Xu L-H. Lamb-dip measurements of ammonia calibration lines in methylamine using a dual-mode CO_2-laser-microwave-sideband spectrometer. J Mol Spectrosc 2008;249:68–70.

[64] Cazzoli G, Dore L, Puzzarini C. The hyperfine structure of the inversion-rotation transition $J_K = 1_0 \leftarrow 0_0$ of NH_3 investigated by Lamb-dip spectroscopy. Astron Astrophys 2009;507:1707–10.

[65] Coy SL, Lehmann KK. Rotational structure of ammonia N-H stretch overtones: five and six quanta bands. J Chem Phys 1986;84:5239–49.

[66] Yurchenko SN, Barber RJ, Yachmenev A, Thiel W, Jensen P, Tennyson J. A variationally computed $T = 300$ K line list for NH_3. J Phys Chem A 2009;113:11845–55.

[67] Yurchenko SN, Barber RJ, Tennyson J. A variationally computed hot line list for NH_3. Mon Not R Astron Soc 2011;413:1828–34.

[68] Huang X, Schwenke DW, Lee TJ. Rovibrational spectra of ammonia. II. Detailed analysis, comparison, and prediction of spectroscopic assignments for $^{14}NH_3$, $^{15}NH_3$, and $^{14}ND_3$. J Chem Phys 2011;134:044321.

[69] Yurchenko SN. A theoretical room-temperature line list for $^{15}NH_3$. J Quant Spectrosc Radiat Transf 2015;152:28–36.

[70] Coles PA, Ovsyannikov RI, Polyansky OL, Yurchenko SN, Tennyson J. Improved potential energy surface and spectral assignments for ammonia in the near-infrared region. J Quant Spectrosc Radiat Transf 2018;219:199–212.

[71] Coles PA, Yurchenko SN, Tennyson J. ExoMol molecular line lists XXXV: a rotation-vibration line list for hot ammonia. Mon Not R Astron Soc 2019;490:4638–47.

[72] Tennyson J, Yurchenko SN. ExoMol: molecular line lists for exoplanet and other atmospheres. Mon Not R Astron Soc 2012;425:21–33.

[73] Tennyson J, Yurchenko SN, Al-Refaie AF, Barton EJ, Chubb KL, Coles PA, et al. The ExoMol database: molecular line lists for exoplanet and other hot atmospheres. J Mol Spectrosc 2016;327:73–94.

[74] Costain CC. An empirical formula for the microwave spectrum of ammonia. Phys Rev 1951;82:108.

[75] Sasada H, Endo Y, Hirota E, Poynter RL, Margolis JS. Microwave and Fourier–transform infrared spectroscopy of the $\nu_4 = 1$ and $\nu_2 = 2$ states of NH_3. J Mol Spectrosc 1992;151:33–53.

[76] Kleiner I, Tarrago G, Brown LR. Positions and intensities in the $3\nu_2/\nu_2 + \nu_4$ vibrational system of $^{14}NH_3$ near 4 µm. J Mol Spectrosc 1995;173:120–45.

[77] Cottaz C, Kleiner I, Tarrago G, Brown LR, Margolis JS, Poynter RL, et al. Line positions and intensities in the $2\nu_2/\nu_4$ vibrational system of $^{14}NH_3$ near 5–7 µm. J Mol Spectrosc 2000;203:285–309.

[78] Cottaz C, Tarrago G, Kleiner I, Brown LR. Assignments and intensities of $^{14}NH_3$ hot bands in the 5- to 8-µm ($3\nu_2 - \nu_2$, $\nu_2 + \nu_4 - \nu_2$) and 4-µm ($4\nu_2 - \nu_2$, $\nu_1 - \nu_2$, $\nu_3 - \nu_2$ and $2\nu_4 - \nu_2$) regions. J Mol Spectrosc 2001;209:30–49.

[79] Sung K, Brown LR, Huang X, Schwenke DW, Lee TJ, Coy SL, et al. Extended line positions, intensities, empirical lower state energies and quantum assignments of NH_3 from 6300 to 7000 cm^{-1}. J Quant Spectrosc Radiat Transf 2012;113:1066–83.

[80] Chen P, Pearson JC, Pickett HM, Matsuura S, Blake GA. Measurements of $^{14}NH_3$ in the $\nu_2 = 1$ state by a solid-state, photomixing, THz spectrometer, and a simultaneous analysis of the microwave, terahertz, and infrared transitions between the ground and ν_2 inversion-rotation levels. J Mol Spectrosc 2006;236:116–26.

[81] Yu S, Pearson JC, Drouin BJ, Sung K, Pirali O, Vervloet M, et al. Submillimeter-wave and far-infrared spectroscopy of high-J transitions of the ground and $\nu_2 = 1$ states of ammonia. J Chem Phys 2010;133:174317.

[82] Pearson J, Yu S, Pearson J, Sung K, Drouin B, Pirali O. Extended measurements and an experimental accuracy effective hamiltonian model for the $3\nu_2$ and $\nu_4 + \nu_2$ states of ammonia. J Mol Spectrosc 2018;353:60–6.

[83] Furtenbacher T, Császár AG. MARVEL: measured active rotational-vibrational energy levels. II. Algorithmic improvements. J Quant Spectrosc Radiat Transf 2012;113:929–35.

[84] Árendás P, Furtenbacher T, Császár AG. On spectra of spectra. J Math Chem 2016;54:806–22.

[85] Császár AG, Czakó G, Furtenbacher T, Mátyus E. An active database approach to complete rotational–vibrational spectra of small molecules. Annu Rep Comput Chem 2007;3:155–76.

[86] Furtenbacher T, Árendás P, Mellau G, Császár AG. Simple molecules as complex systems. Sci Rep 2014;4:4654.

[87] Furtenbacher T, Szabó I, Császár AG, Bernath PF, Yurchenko SN, Tennyson J. Experimental energy levels and partition function of the $^{12}C_2$ molecule. Astrophys J Suppl 2016;224:44.

[88] McKemmish LK, Masseron T, Sheppard S, Sandeman E, Schofield Z, Furtenbacher T, et al. MARVEL analysis of the measured high-resolution spectra of $^{48}Ti^{16}O$. Astrophys J Suppl 2017;228:15.

[89] McKemmish LK, Borsovszky J, Goodhew KL, Sheppard S, Bennett AFV, Martin ADJ, et al. MARVEL analysis of the measured high-resolution spectra of $^{90}Zr^{16}O$. Astrophys J 2018;867:33.

[90] Darby-Lewis D, Shah H, Joshi D, Kahn F, Kauwo M, Sethi N, et al. MARVEL analysis of the measured high-resolution spectra of ^{14}NH. J Mol Spectrosc 2019;362:69–76.

[91] Furtenbacher T, Horváth M, Koller D, Sólyom P, Balogh A, Balogh I, et al. MARVEL analysis of the measured high-resolution rovibronic spectra and definitive ideal-gas thermochemistry of the $^{16}O_2$ molecule. J Phys Chem Ref Data 2019;48:023101.

[92] Furtenbacher T, Szidarovszky T, Mátyus E, Fábri C, Császár AG. Analysis of the rotational–vibrational states of the molecular ion H_3^+. J Chem Theory Comput 2013;9:5471–8.

[93] Furtenbacher T, Szidarovszky T, Fábri C, Császár AG. MARVEL analysis of the rotational–vibrational states of the molecular ions H_2D^+ and D_2H^+. Phys Chem Chem Phys 2013;15:10181–93.

[94] Tennyson J, Bernath PF, Brown LR, Campargue A, Carleer MR, Császár AG, et al. IUPAC critical evaluation of the rotational-vibrational spectra of water vapor. Part I. Energy levels and transition wavenumbers for $H_2{}^{17}O$ and $H_2{}^{18}O$. J Quant Spectrosc Radiat Transf 2009;110:573–96.

[95] Tennyson J, Bernath PF, Brown LR, Campargue A, Carleer MR, Császár AG, et al. IUPAC critical evaluation of the rotational-vibrational spectra of water vapor. Part II. Energy levels and transition wavenumbers for $HD^{16}O$, $HD^{17}O$, and $HD^{18}O$. J Quant Spectrosc Radiat Transf 2010;111:2160–84.

[96] Tennyson J, Bernath PF, Brown LR, Campargue A, Carleer MR, Császár AG, et al. IUPAC critical evaluation of the rotational-vibrational spectra of water vapor. Part III. Energy levels and transition wavenumbers for $H_2{}^{16}O$. J Quant Spectrosc Radiat Transf 2013;117:29–80.

[97] Tennyson J, Bernath PF, Brown LR, Campargue A, Császár AG, Daumont L, et al. IUPAC critical evaluation of the rotational-vibrational spectra of water vapor. Part IV. Energy levels and transition wavenumbers for $D_2{}^{16}O$, $D_2{}^{17}O$ and $D_2{}^{18}O$. J Quant Spectrosc Radiat Transf 2014;142:93–108.

[98] Tennyson J, Bernath PF, Brown LR, Campargue A, Császár AG, Daumont L, et al. A database of water transitions from experiment and theory (IUPAC Technical Report). Pure Appl Chem 2014;86:71–83.

[99] Tóbiás R, Furtenbacher T, Császár AG, Naumenko OV, Tennyson J, Flaud J-M, et al. Critical evaluation of measured rotational-vibrational transitions of four sulphur isotopologues of $S^{16}O_2$. J Quant Spectrosc Radiat Transf 2018;208:152–63.

[100] Chubb KL, Naumenko OV, Keely S, Bartolotto S, MacDonald S, Mukhtar M, et al. MARVEL analysis of the measured high-resolution rovibrational spectra of H_2S. J Quant Spectrosc Radiat Transf 2018;218:178–86.

[101] Wang Y, Owens A, Tennyson J, Yurchenko SN. MARVEL analysis of the measured high-resolution rovibronic spectra of the calcium monohydroxide radical (CaOH). Astrophys J Suppl 2020.

[102] Chubb KL, Joseph M, Franklin J, Choudhury N, Furtenbacher T, Császár AG, et al. MARVEL analysis of the measured high-resolution spectra of C_2H_2. J Quant Spectrosc Radiat Transf 2018;204:42–55.

[103] Fábri C, Mátyus E, Furtenbacher T, Nemes L, Mihály B, Zoltáni T, et al. Variational quantum mechanical and active database approaches to the rotational-vibrational spectroscopy of ketene, H_2CCO. J Chem Phys 2011;135:094307.

[104] Bunker PR, Jensen P, editors. Molecular symmetry and spectroscopy, 2nd ed.. NRC Research Press, Ottawa, Ontario, Canada; 1998.

[105] Urban Š, D'Cunha R, Narahari Rao K, Papoušek D. The $\Delta k = \pm 2$ "forbidden band" and inversion-rotation energy levels of ammonia. Can J Phys 1984;62:1775–91.

[106] Tóbiás R, Furtenbacher T, Simkó I, Császár AG, Diouf ML, Cozijn FMJ, et al. Spectroscopic-network-assisted precision spectroscopy and its application to water. Nature Comm 2020;11:1708.

[107] Down MJ, Hill C, Yurchenko SN, Tennyson J, Brown LR, Kleiner I. Re-analysis of ammonia spectra: updating the HITRAN $^{14}NH_3$ database. J Quant Spectrosc Radiat Transf 2013;130:260–72.

[108] Huang X.. Xinchuan Huang SETI webpage; 2013. http://huang.seti.org/.

[109] Cohen EA, Poynter RL. The microwave spectrum of $^{14}NH_3$ in the $\nu = 000^01^1$ state. J Mol Spectrosc 1974;53:131–9.

[110] Poynter RL, Kakar RK. The microwave frequencies, line parameters, and spectral constants for $^{14}NH_3$. Astrophys J Suppl 1975;29:87–96.

[111] Tanaka K, Endo Y, Hirota E. Submillimeter-wave spectrum of $k = \pm 1 \leftarrow \mp 2$ transitions of NH_3. Chem Phys Lett 1988;146:165–8.

[112] Sasada H, Hasegawa Y, Amano T, Shimizu T. High-resolution infrared and microwave spectroscopy of the ν_4 and $2\nu_2$ bands of $^{14}NH_3$ and $^{15}NH_3$. J Mol Spectrosc 1982;96:106–30.

[113] Fichoux H, Khelkhal M, Rusinek E, Legrand J, Herlemont F, Urban Š. Double resonance sub-Doppler study of the allowed and $\Delta K = -3$ forbidden $Q(3,3)$ transitions to the ν_2 vibrational state of $^{14}NH_3$. J Mol Spectrosc 1998;192:169–78.

[114] Cohen EA. The ν_4 state inversion spectra of $^{15}NH_3$ and $^{14}NH_3$. J Mol Spectrosc 1980;79:496–501.

[115] Drouin BJ, Yu S, Pearson JC, Gupta H. Terahertz spectroscopy for space applications: 2.5–2.7 THz spectra of HD, H_2O and NH_3. J Mol Struct 2011;1006:2–12.

[116] Krupnov AF, Tretyakov MY, Bogey M, Bailleux S, Walters A, Delcroix B, et al. Microwave measurements of $J = 2 \leftarrow 1$, $K = 0, 1$ ammonia transitions at 1.215 THz. J Mol Spectrosc 1996;176:442–3.

[117] Belov SP, Urban Š, Winnewisser G. Hyperfine structure of rotation-inversion levels in the excited ν_2 state of ammonia. J Mol Spectrosc 1998;189:1–7.

[118] Urban Š, Herlemont F, Khelkhal M, Fichoux H, Legrand J. High-accuracy determination of the frequency and quadrupole structure of the $sP(1,0)$ and $aR(0,0)$ transitions to the ν_2 state of $^{14}NH_3$. J Mol Spectrosc 2000;200:280–2.

[119] Guinet M, Jeseck P, Mondelain D, Pepin I, Janssen C, Camy-Peyret C, et al. Absolute measurements of intensities, positions and self-broadening coefficients of R branch transitions in the ν_2 band of ammonia. J Quant Spectrosc Radiat Transf 2011;112:1950–60.

[120] Brown LR, Toth RA. Comparison of the frequencies of NH_3, CO_2, H_2O, N_2O, CO, and CH_4 as infrared calibration standards. J Opt Soc Am B 1985;2:842–56.

[121] Sasada H, Schwendeman RH, Magerl G, Poynter RL, Margolis JS. High-resolution spectroscopy of the $\nu_2 = 2a \leftarrow \nu_2 = 1s$ band of $^{14}NH_3$. J Mol Spectrosc 1986;117:317–30.

[122] Urban Š, Tu N, Narahari Rao K, Guelachvili G. Analysis of high-resolution Fourier transform spectra of $^{14}NH_3$ at 2.3 μm. J Mol Spectrosc 1989;133:312–30.

[123] Sattler JP, Miller LS, Worchesky TL. Diode laser heterodyne measurements on $^{14}NH_3$. J Mol Spectrosc 1981;88:347–51.

[124] Urban Š, Papoušek D, Kauppinen J, Yamada K, Winnewisser G. The ν_2 band of $^{14}NH_3$: a calibration standard with better than 1×10^{-4} cm^{-1} precision. J Mol Spectrosc 1983;101:1–15.

[125] Poynter RL, Margolis JS. The ν_2 spectrum of NH_3. Mol Phys 1984;51:393–412.

[126] Chu Z, Chen L, Cheo PK. Absorption spectra of NH_3 using a microwave-sideband CO_2-laser spectrometer. J Quant Spectrosc Radiat Transf 1994;51:591–602.

[127] Hillman JJ, Jennings DE, Faris JL. Diode laser–CO_2 laser heterodyne spectrometer: measurement of $2sQ(1, 1)$ in $2\nu_2 - \nu_2$ of NH_3. Appl Opt 1979;18:1808–11.

[128] Urban Š, Špirko V, Papoušek D, Kauppinen J, Belov SP, Gershtein LI, et al. A simultaneous analysis of the microwave, submillimeterwave, far infrared, and infrared-microwave two-photon transitions between the ground and ν_2 inversion-rotation levels of $^{14}NH_3$. J Mol Spectrosc 1981;88:274–92.

[129] Weber WH. Laser-Stark spectrum of NH_3 with the CO laser: determination of the ground state dipole moment. J Mol Spectrosc 1984;107:405–16.

[130] Guelachvili G, Abdullah AH, Tu N, Narahari Rao K, Urban Š, Papoušek D. Analysis of high-resolution Fourier-transform spectra of $^{14}NH_3$ at 3.0 μm. J Mol Spectrosc 1989;133:345–64.

[131] Pine AS, Dang-Nhu M. Spectral intensities in the ν_1 band of NH_3. J Quant Spectrosc Radiat Transf 1993;50:565–70.

[132] Brown LR, Margolis JS. Empirical line parameters of NH_3 from 4791 to 5294 cm^{-1}. J Quant Spectrosc Radiat Transf 1996;56:283–94.

[133] Fabian M, Yamada KMT. Absolute intensity of the $NH_3\nu_2$ band. J Mol Spectrosc 1999;198:102–9.

[134] Kleiner I, Brown LR, Tarrago G, Kou Q-L, Picqué N, Guelachvili G, et al. Positions and intensities in the $2\nu_4/\nu_1/\nu_3$ vibrational system of $^{14}NH_3$ near 3 μm. J Quant Spectrosc Radiat Transf 1999;193:46–71.

[135] Földes T, Golebiowski D, Herman M, Softley TP, Di Lonardo G, Fusina L. Low-temperature high-resolution absorption spectrum of $^{14}NH_3$ in the $\nu_1 + \nu_3$ band region (1.51 μm). Mol Phys 2014;112:2407–18.

[136] Urban Š, D'Cunha R, Manheim J, Narahari Rao K. High-J transitions in the ν_2 bands of $^{14}NH_3$ and $^{15}NH_3$. J Mol Spectrosc 1986;118:298–309.

[137] Nereson N. Diode laser measurements of NH_3 absorption lines around 10.6 μm. J Mol Spectrosc 1978;69:489–93.

[138] Papousek D, Urban S, Spirko V, Rao KN. The $\Delta k = \pm 2$ and $\Delta k = \pm 3$ forbidden transitions in the vibrational-rotational spectra of symmetric top molecules NH_3 and H_3O^+. J Mol Spectrosc 1986;141:361–6.

[139] Brown LR, Peterson DB. An empirical expression for linewidths of ammonia from far-infrared measurements. J Mol Spectrosc 1994;168:593–606.

[140] Angstl R, Finsterholzl H, Frunder H, Illig D, Papoušek D, Pračna P, et al. Fourier transform and CARS spectroscopy of the ν_1 and ν_3 fundamental bands of $^{14}NH_3$. J Mol Spectrosc 1985;114:454–72.

[141] Zobov NF, Shirin SV, Ovsyannikov RI, Polyansky OL, Yurchenko SN, Barber RJ, et al. Analysis of high temperature ammonia spectra from 780 to 2100 cm^{-1}. J Mol Spectrosc 2011;269:104–8.

[142] Down MJ, Hill C, Yurchenko SN, Tennyson J, Brown LR, Kleiner I. Re-analysis of ammonia spectra: updating the HITRAN $^{14}NH_3$ database. J Quant Spectrosc Radiat Transf 2013;130:260–72.
[143] Cermák P, Hovorka J, Veis P, Cacciani P, Cosléou J, Romh JE, et al. Spectroscopy of $^{14}NH_3$ and $^{15}NH_3$ in the 2.3 µm spectral range with a new VECSEL laser source. J Quant Spectrosc Radiat Transf 2014;137:13–22.
[144] Hermanussen J, Bizzarri A, Baldacchini G. Diode laser measurements of ammonia absorption lines over the range 620–740 cm^{-1}. J Mol Spectrosc 1986;119:291–8.
[145] Li L, Lees RM, Xu L-H. External cavity tunable diode laser spectra of the $\nu_1 + 2\nu_4$ stretch-band combination bands of $^{14}NH_3$ and $^{15}NH_3$. J Mol Spectrosc 2007;243:219–26.
[146] Lees RM, Li L, Xu L-H. New VISTA on ammonia in the 1.5 µm region: assignments for the ν_3+2ν_4 bands of $^{14}NH_3$ and $^{15}NH_3$ by isotopic shift labeling. J Mol Spectrosc 2008;251:241–51.
[147] Dietiker P, Milogyadov E, Quack M, Schneider A, Seyfang G. Two photon IR-laser induced population transfer in NH_3 – First steps to measure parity violation in chiral molecules. In: Stock D, Wester R, Scheier P, editors. Proceedings of the 19th symposium on atomic, cluster and surface physics 2014 (SASP 2014). Innsbruck University Press, Insbruck; 2014. p. p..
[148] Urban Š, Špirko V, Papoušek D, McDowell RS, Nereson NG, Belov SP, et al. Coriolis and *l*-type interactions in the ν_2, $2\nu_2$, and ν_4 states of $^{14}NH_3$. J Mol Spectrosc 1980;79:455–95.
[149] Helminger P, De Lucia FC, Gordy W. Rotational spectra of NH_3 and ND_3 in the 0.5-mm wavelength region. J Mol Spectrosc 1971;39:94–7.
[150] Urban Š, Misra P, Narahari Rao K. The $\nu_1 + \nu_2$ and $\nu_1 + \nu_2 - \nu_2$ bands of $^{14}NH_3$ and $^{15}NH_3$. J Mol Spectrosc 1985;114:377–94.
[151] Lundsberg-Nielsen L, Hegelund F, Nicolaisen FM. Analysis of the high--resolution spectrum of ammonia ($^{14}NH_3$) in the near-infrared region, 6400–6900 cm^{-1}. J Mol Spectrosc 1993;162:230–45.
[152] Petersen JC, Hald J. Microwave optical double resonance spectroscopy of ammonia in a hollow-core fiber. Opt Express 2010;18:7955–64.
[153] Berden G, Peeters R, Meijer G. Cavity-enhanced absorption spectroscopy of the 1.5 µm band system of jet-cooled ammonia. Chem Phys Lett 1999;307:131–8.
[154] Xu L-H, Liu Z, Yakovlev I, Tretyakov MY, Lees RM. External cavity tunable diode laser NH_3 spectra in the 1.5 µm region. Infrared Phys Techn 2004;45:31–45.
[155] Barton EJ, Yurchenko SN, Tennyson J, Clausen S, Fateev A. High-resolution absorption measurements of NH_3 at high temperatures: 500 – 2100 cm^{-1}. J Quant Spectrosc Radiat Transf 2015;167:126–34.
[156] Beale CA, Wong A, Bernath P. Infrared transmission spectra of hot ammonia in the 4800–9000 cm^{-1} region. J Quant Spectrosc Radiat Transf 2020;246:106911.
[157] Polyansky OL, Ovsyannikov RI, Kyuberis AA, Lodi L, Tennyson J, Yachmenev A, et al. Calculation of rotation-vibration energy levels of the ammonia molecule based on an *ab initio* potential energy surface. J Mol Spectrosc 2016;327:21–30.
[158] Gordon IE, et al. The HITRAN 2016 molecular spectroscopic database. J Quant Spectrosc Radiat Transf 2017;203:3–69.
[159] National Academies of Sciences Engineering, and Medicine. Frequency Allocations and Spectrum Protection for Scientific Uses, 2nd edition. The National Academies Press, Washington D.C.; 2015.
[160] Birkby JL. Spectroscopic direct detection of exoplanets. Handbook of Exoplanets 2018:1485–508.
[161] Lutz BL, Owen T. Visible bands of ammonia - band strengths, curves of growth, and the spatial-distribution of ammonia on Jupiter. Astrophys J 1980;235:285–93.
[162] Irwin PGJ, Bowles N, Braude AS, Garland R, Calcutt S, Coles PA, et al. Analysis of gaseous ammonia (NH_3) absorption in the visible spectrum of Jupiter - Update. Icarus 2019;321:572–82.